Solvent free highly efficient Metathesis and development of biobased polyesters from waste and renewable lipids

by

Rehan Ali Pradhan

A thesis submitted in partial fulfillment of the requirements for the degree of

Master of Science

in

BIORESOURCE TECHNOLOGY

Department of Agricultural, Food and Nutritional Science

University of Alberta

Abstract

Linear economy is a traditional way of making materials, for instance utilization of fossil fuel to develop plastics that finally end-up into landfills and oceans posing threat to the existence of marine life and disrupting natural harmony and co-existence. On the other hand, circular economy is an emerging concept, which induces circular flow of materials that minimizes the reliance on virgin materials and treat waste as the useful feedstock. An attempt was made to adopt the principle of circular economy to develop biobased materials from used waste lipids taken/extracted from used cooking oil and spent hen and compared with canola oil without extensive purification.

This thesis firstly reports the synthesis of polymer precursors from these waste lipidic feedstocks using microwave-assisted solvent-less ethenolysis. The turnover numbers (TONs) of the catalyst were significantly improved through optimization of catalyst/feedstock system. Excellent turnover number values were demonstrated for the ethenolysis of Canola Oil Esters (TONs= 92000), Used-Cooking Oil Esters (TONs= 78080) and Chicken Fat Esters (TONs=21820). Moreover, the synthesis method involved no use of toxic solvents together with the sheer elimination of extensive purification step for substrates and catalysts. Secondly, the ethenolyzed products were separated into non-functionalized olefinic and functionalized olefinic (ester and diester) components, and the isolated diester component was further subjected to condensation polymerization to produce bio-based polyesters. The synthesized product was characterized and investigated using different techniques including Nuclear Magnetic Resonance (NMR), Attenuated Total Reflectance-Fourier Transformed Infrared Spectroscopy (ATR-FTIR), Gas chromatography-Mass Spectroscopy (GC-MS), Gas Chromatography-Flame Ionization Detector (GC-FID), Differential Scanning Calorimetry (DSC), Thermogravimetric Analysis (TGA) and Universal Testing Machine (UTM). The processed polyester film displayed tensile strength of 2.44 MPa and modulus of elasticity of

137.6 MPa. Efforts were also made to introduce 10-20% of aromatic diol from lignocellulosic biomass to further improve thermomechanical properties. These results indicate potential utilization of waste lipidic resources to substitute conventional petroleum resources.

The present work, based on rapid synthesis and greener approach, could open new opportunities for sustainable production of bio-based polymer precursors and development of polyesters for utilization in soft packaging and other applications.

Preface

This work was performed between 2018 and 2020 in

Utilization Of Lipids - Polymers/Materials Chemistry Research Group at the University of Alberta

under the supervision of Dr. Aman Ullah, who helped with the study conception.

Chapters 2 has been published as Short communication: "Solvent-free rapid ethenolysis of fatty

esters from spent hen and other lipidic feedstock with high turnover numbers", in Journal of

Industrial and Engineering Chemistry (2020) https://doi.org/10.1016/j.jiec.2020.01.002. In this

work, I performed experiments, collected, and analyzed the data, and prepared manuscript under

supervision and assistance of Dr. Aman Ullah. Dr. Arshad assisted me during experiments and

further edited the manuscript before submission.

Dedication

I would like to dedicate this work to my parents, Irfan and Gulshan; and my sisters, Sadaf and Saher, my love, Arzoo and my son, Shazaan for all their support and love in this journey.

Last but not the least, to all the intrepid souls who contribute in bringing peace and harmony in this world.

Acknowledgements

First, I would like to express my sincere gratitude to my supervisor, Dr. Aman Ullah. I was a MITACS visiting scholar in 2014 and his positive influence brought me back to the University of Alberta to pursue my Master studies under his supervision. He always provided moral support and encouragement. I learned from him, passion and sincere commitment towards my goals. It was an exciting and a great learning opportunity to attend his course AFNS 510 on Renewable Biomaterials. I would also like to thank Dr. Johnathan Curtis and Dr. John Veinot who, through their courses, enabled me to understand the principles of advanced chemical analysis and nano-technological techniques.

I am also thankful to Dr. Muhammad Arshad (our group) and Ereddad Kharraz for their guidance and help in using different pieces of equipment. I would also like to extend thanks to Dr. Kelvin Lien (food science technologist AFNS), Dr. Mohammad Hossein Tavassoli Kafrani and Anna Magdalena Hubmann (Dr. Curtis group). In addition, a thank you to AFNS staff, including Urmila Basu, Eduardo Rodriguez for their kindness of supplying materials, suggestions and convenience during my whole program.

I want to acknowledge social support from my friends and colleagues in the office, Muhammad Safder, Muhammad Zubair, Reza Ahmadi, Xiaohua Cai, Yanet Rodriguez Herrero, Punita Upadhyay, Irum Zahara, Karen Lopez-Camas, Saadman Sakib Rahman and Shifa Dinesh.

Finally, I would like to acknowledge that this research was conducted at the University of Alberta, which is located on Treaty 6 territory, traditional meeting ground and home for many Indigenous Peoples, including Cree, Saulteaux, Niisitapi (Blackfoot), Métis, and Nakota Sioux.

Table of Contents

List of Figures

List of Schemes

List of Tables

List of Abbreviations and Symbols

ADA   Aliphatic dicarboxylic acids

Al_2O_3 Aluminium Oxide

ATR-FTIR   Attenuated Total Reflectance- Fourier Transformed Infrared Spectroscopy

CE   Circular Economy

CF   Chicken Fat

CO   Canola Oil

CO_2 Carbon Dioxide

DEG   Diethylene Glycol

DMT   Dimethyl Terephthalate

DSC   Differential Scanning Calorimetry

EG   Ethylene Glycol

FDCA   2, 5-furandicarboxylic acid

G1   Grubbs 1st Generation catalyst

G2   Grubbs 2nd Generation catalyst

GC-FID   Gas Chromatography-Flame Ionization Detector

GC-MS   Gas Chromatography-Mass Spectrometry

GHz   Gigahertz

GPC   Gel Permeation Chromatography

H_3PO_4 Phosphoric Acid

HCl   Hydrochloric acid

HG1   Hoveyda-Grubbs 1st Generation catalyst

HG2   Hoveyda-Grubbs 2nd Generation catalyst

kW   kilowatt

LAOs   Linear α-olefins

MHz   megahertz

NHC   N-Heterocyclic Carbene

NMR   Nuclear Magnetic Resonance

PBS   Poly (butylene succinate)

PEEK	Poly (ether ether ketone)
PEF	Poly (ethylene 2, 5-furandicarboxylate)
PET	Poly (ethylene terephthalate)
PLA	Poly (lactic acid)
RH	Relative Humidity
TEP	Triethyl Phosphate
T_g	Glass Transition Temperature
TGA	Thermogravimetric Analysis
THF	Tetrahydrofuran
TLC	Thin Layer Chromatography
T_m	Melting Temperature
TMP	Trimethyl Phosphate
TOF	Turnover Frequency
TONs	Turnover Numbers
TPA	Terephthalic Acid
TPP	Triphenyl Phosphate
UCO	Used Cooking Oil

Chapter 1: Introduction

1.1 Current challenges of Polymer industry

Polymers comprise about 40% of the output of the global chemical sector(Ray & Miglani, 2018), which is the largest industrial energy consumer and the third largest industrial emitter of carbon dioxide. There is a tremendous amount of energy required at each stage of extraction, production and distribution of polymer resins. Moreover, most of the plastics end up in landfills after use, and unfortunately it takes thousands of years(Gautam & Caetano, 2017) for plastic to decompose. Resource scarcity, climate change and social imbalances are few of the inevitable challenges that the global civilization is experiencing in the twenty-first century. In the recent years, efforts have been made to overcome the problem of resource scarcity by developing bio-based polymers from renewable sources such as terpenes(Ciriminna et al., 2014; Gandini, 2011; Wilbon et al., 2013), carbon dioxide(Ellis et al., 2014; Hauenstein et al., 2016; Lee et al., 2012; Ren et al., 2009), vegetable oils(Maisonneuve et al., 2013; Meier et al., 2007; Stempfle et al., 2016), proteins(Duan et al., 2018; Dutta, 2016) and carbohydrates(Auras et al., 2004; Inkinen et al., 2011).
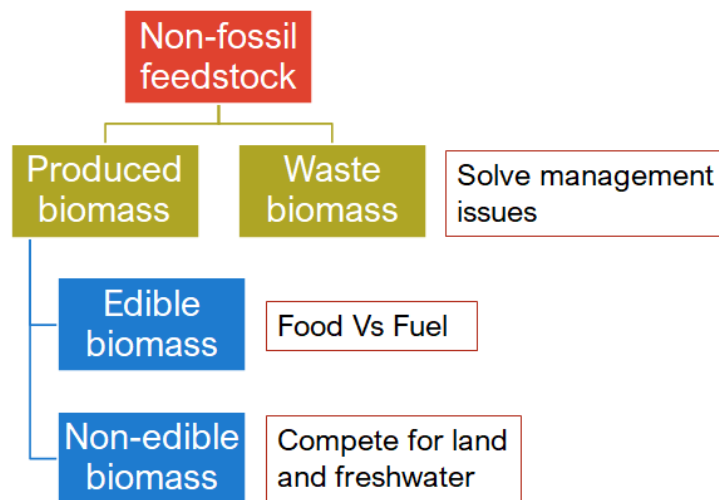
Figure 1.1: Flowchart showcasing various types of biomass resources used to produce polymers

Biomass can be broadly classified into two types namely produced biomass and waste biomass as illustrated in Figure 1.1. Produced biomass consist of edible and non-edible biomass like corn, sugarcane, wood etc. On the other hand, waste biomass includes industrial wastes and residues like used cooking oil, spent hen, chicken feathers to name a few. There are inherent challenges associated with the use of edible biomass such as threatening of the global food security. Additionally, the utilization of non-edible biomass requires land freshwater for its cultivation which adds to energy and resource expenditure. The problem can be solved holistically by utilizing waste as a feedstock, employing waste to energy concept and regenerating waste to make useful products. In the next section, various concepts and methodology that form the basis of this research are highlighted and discussed elaborately.

1.2 Concept of Circular economy

Circular Economy (CE) is an emerging concept which induces circular flow of material to minimize the reliance on virgin materials and promote consumption of secondary materials. The goal is to address the challenges associated with resource shortage and waste disposal, and thereby achieve sustainability in terms of social, economic and environmental aspects. This model contrasts with the linear economy in its objectives of maintaining value (not to create value added), optimising stock management (not flows) and improving upon the efficiency of using goods (not of producing goods)(Stahel, 2019). Figure 1.2 illustrates linearity of the conventional model (take, make, dispose) in contrast to the circular model of production.

It must be emphasized that materials need to be both recoverable and renewable in order to maintain its cyclic regeneration and circular use. Recoverability means that the product formed from the material can be collected after scrapping, such as glass and paper. Conversely, products such as inks and detergent get dissipated into the environment after being used and possess zero

recoverability, and they are difficult to recycle. Renewability means that wastes maintain their original basic properties after going through regeneration. Bio-based materials derived from renewable lipidic wastes manifest these attributes of recoverability and renewability and thereby endorse the principle of circular economy.
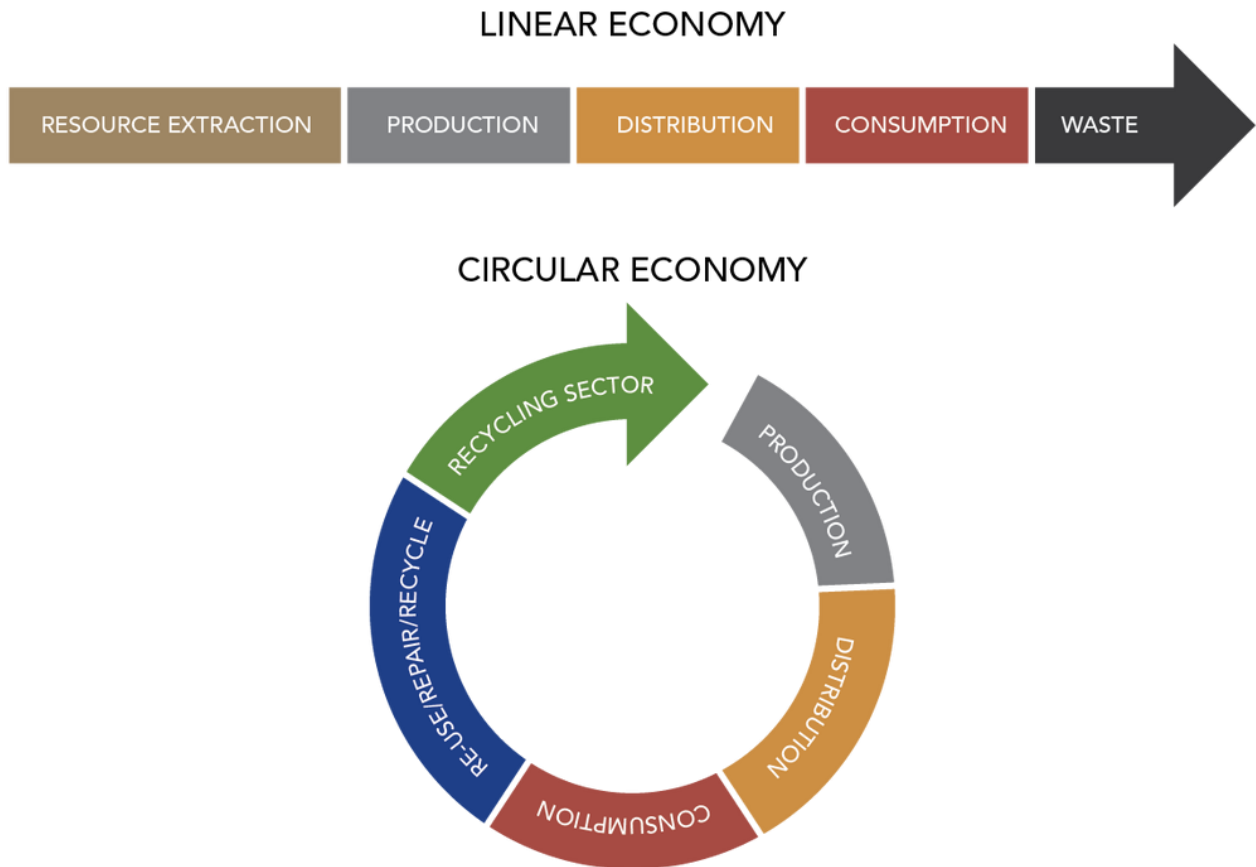
Figure 1.2: Linear and Circular economy model for resources from extraction to end-of-life

1.2.1 Difference between bioeconomy and circular economy

Both approaches focus on a low-carbon economy, economic growth, innovation and new technologies, but the circular economy responds to a broader set of factors including design, recycling and reuse. While use of edible crops for biofuel production fall under the roof of bioeconomy, it doesn't support circular economy holistically as additional resources (Land, water)

are required that increases the demand for energy during production and resource extraction. On the other hand, waste and industrial residues require no land and avoid landfill and management issues, thereby holistically complementing the principles of circular economy. Therefore, a circular economy strategy holds the potential to address a more comprehensive set of environmental challenges and it is disruptive to the current model of the economy. Nevertheless, bioeconomy is an important component of circular economy activities in Canada, especially where biotechnology can enable the transformation of biomass that would otherwise not be fully utilized into useful products.

1.3 Microwave enhanced material synthesis

Microwave radiation are the kind of electromagnetic waves which have the frequencies of 300 MHz to 300 GHz (corresponding wavelength: 1 mm to 1 m). These possess higher energy than radio waves but lower energy than infrared waves. Most of the microwave used currently have a standard working frequency of 2.45 GHz(Bogdal & Prociak, 2008). These radiations can generate localized heating inside the surface of the material which is not achieved in conventional heating as shown in Figure 1.3. Nevertheless, these radiations interact differently with different class of materials as outlined in Figure 1.4. The interaction of microwave with conductors leads to reflection from its surface. For insulators with good dielectric properties (quartz glass, ceramics), microwave radiation can penetrate the material without any absorption. However, in the case of insulators with lossy dielectric properties, microwaves can be absorbed by the material that eventually get transformed into heat. Polar organic solvents (acetonitrile, ethyl alcohol) possess relatively high values of dielectric constants and, in turn, can be heated by dielectric heating mechanism under microwave irradiation. Polar solvents interact strongly with microwave and absorb most of the energy thereby limiting the energy transport to internal parts of the mixture as

also observed in the conventional heating. However, addition of small amount of polar solvent along with non-polar solvents can lead to dramatic rise in temperature and thereby improve microwave absorption as well as temperature homogeneity of the sample. Nonpolar organic solvents (i.e., benzene, carbon tetrachloride, n-hexane) possess low dielectric constants and, in fact, show negligible heating effects under microwave irradiation. The symmetrical structure of n-hexane renders it ineffective to possess a dipole moment and hence it does not absorb microwaves(Bogdal & Prociak, 2008). It must be noted that penetration depth is also crucial along with microwave absorption to harness the advantage of microwave heating. Otherwise only some parts (outer layers) of the reaction mixture would interact with microwaves to generate heat, and the remaining part of the mixture would be heated by heat convection and/or conduction mechanism. Dielectric constant of the material is the function of temperature as well as interacting wave-frequency. For example, the molecules of water exhibit highest heating effectiveness at 20 GHz. Even though maximum heating (maximum heat loss) is achieved at this frequency, the uniformity in heating is compromised. Skin effect is observed where, the microwaves are absorbed in the outer region of the material and penetrate only a short distance. The penetration depth is also affected by temperature parameter. The penetration depth of microwave radiation towards water is 1.4 cm at 25°C and 5.7 cm at 95°C(Bogdal & Prociak, 2008).
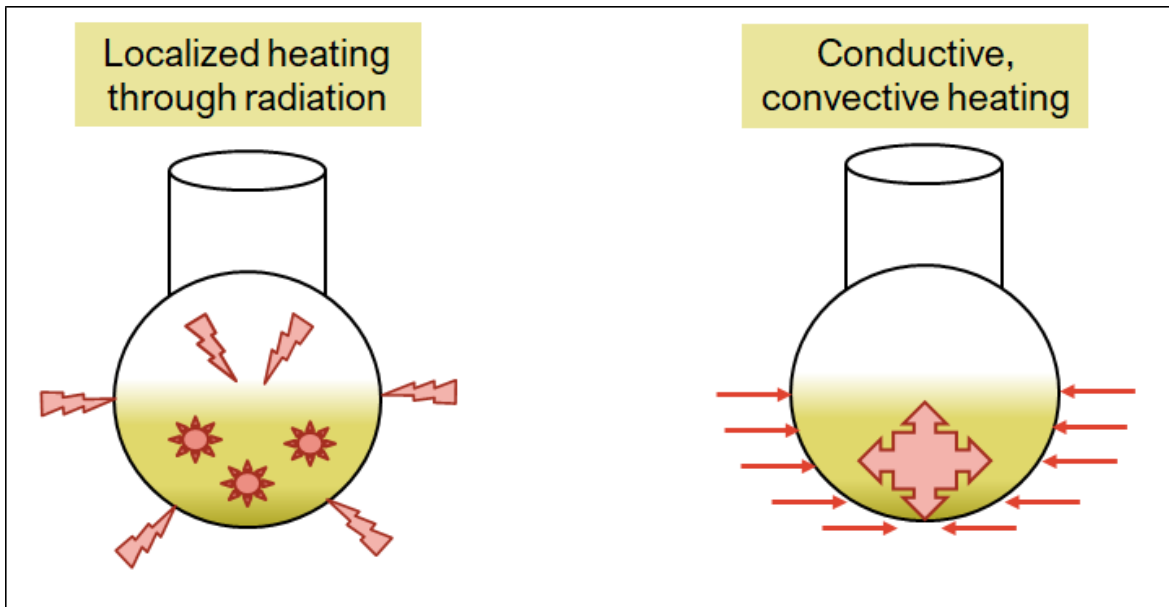
Figure 1.3: Localized and surface heating phenomena in microwave and conventional process

There are several advantages offered by microwave heating over conventional heating. Rapid start up and shut down can be achieved thereby avoiding the thermal lags associated with conduction and/or convection which contribute towards energy savings during microwave processing. Time and energy savings are the crucial parameters which not only governs the process efficiency but also the economics of any system. In comparison to conventional heating, microwave offers equivalent yield of final products in a tenth part (or even smaller) of the total time. Apart from accelerated reaction with microwave radiation, other advantages include improved product uniformity, reduced extrusion-line length, reduced scrap, and improved cleanliness and environmental sustainability compared with steam autoclaves, hot air, slat batch, or fluid bed heating processes. Selective heating can be achieved based on dielectric properties of the material and this can safeguard sensitive additives from detrimental consequences of degradation.
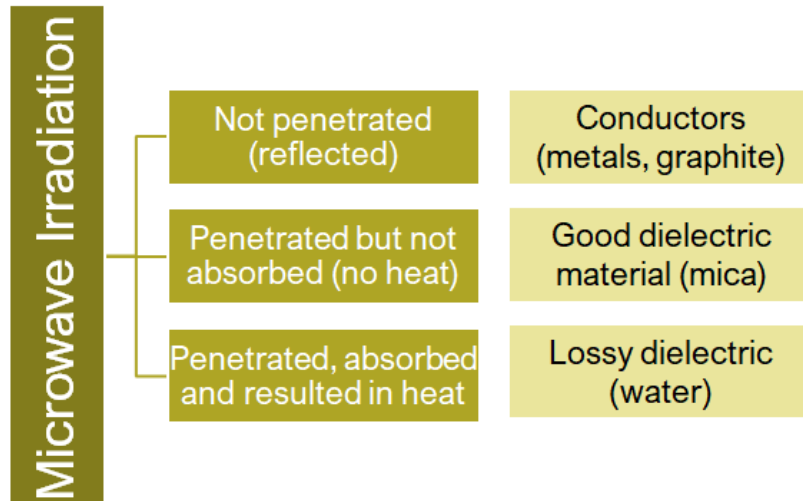
Figure 1.4: Interaction of microwave radiation with different class of materials

However, one of the major disadvantages of microwave in comparison to conventional heating is high initial capital cost. Moreover, magnetron which forms the major component of microwave possess maximum power of 100 kW. For industrial applications, additional energy can be generated by utilizing multiple sources. High power magnetron (915 MHz) manifest plug to product efficiency between 80% - 87%, while standard microwave (2.45 GHz) showcase efficiency between 50% - 72%(Bogdal & Prociak, 2008). The feasibility of using microwave ultimately depends upon several variables such as local variations in energy costs, environmental laws, labor costs along with the properties of finished materials or parts, improvements in yield or productivity, and the markets for the products.

1.4 Olefin Metathesis for monomer production

Olefin metathesis involves double displacement reaction between the reacting species. It can take place within the same species(self-metathesis) or with another reacting component (cross metathesis) as depicted in the following scheme.
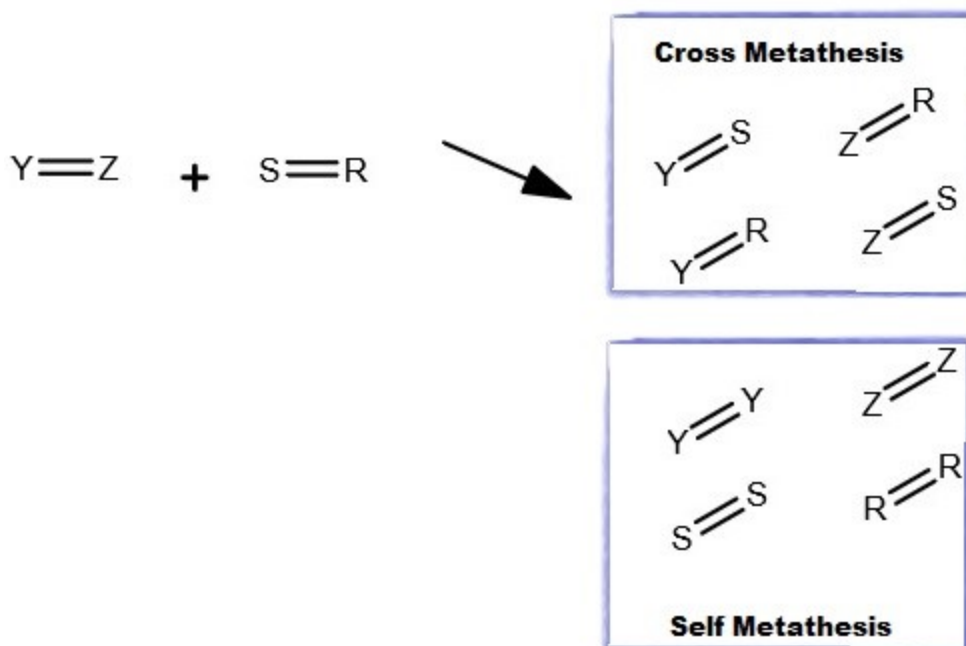
Scheme 1.1: Schematic diagram for olefin metathesis

Cross metathesis reaction with ethylene is called ethenolysis. During ethenolysis, a metal-methylidene specie is formed which reacts with unsaturated hydrocarbon to yield terminal unsaturated specie. Chauvin mechanism proposed for the ethenolysis is shown in Scheme 1.2. The terminal alkene formed can serve as the potential precursor for further polymerization to obtain specialty chemicals. Side products are also formed during the reaction which can be minimized by incorporating suitable catalyst, appropriate temperature and pure substrate. The difference in physical and chemical conditions can alter the reaction time, yield, selectivity, turnover number (TON, the number of moles of substrate that a mole of catalyst can convert before becoming inactivated) which influences the efficacy of the reaction. For economic viability, metathesis turnover number must be greater than 50,000(Burdett et al., 2004). This commercial limit is set by Dow Chemical Company, based on the price of homogenous catalyst.
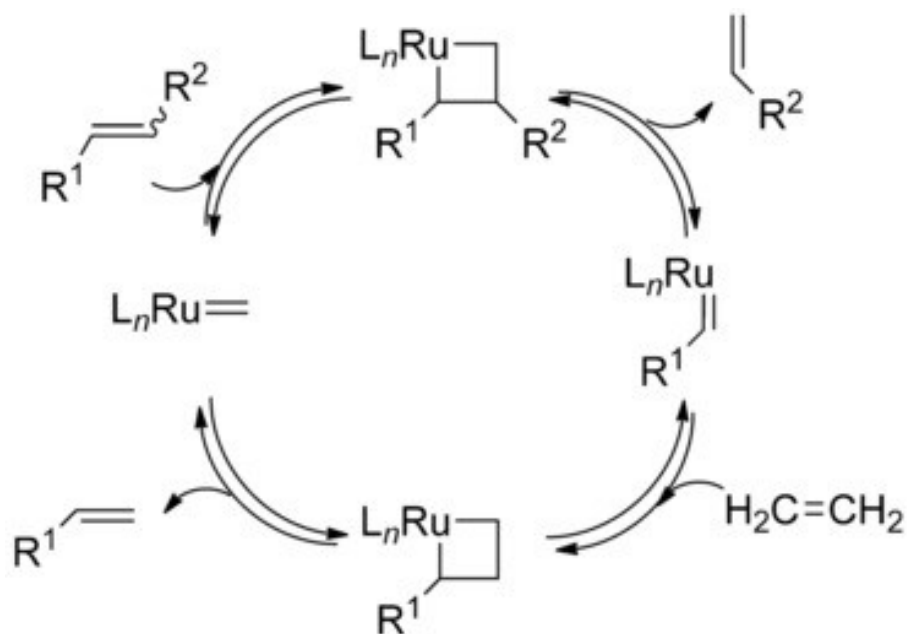
Scheme 1.2. Chauvin mechanism for ethenolysis {Adapted with permission from Ethenolysis: A Green Catalytic Tool to Cleave Carbon–Carbon Double Bonds. Copyright © 2016, Wiley (Bidange et al., 2016).

Oleochemicals derived from vegetable oils have been widely used in commercial applications such as cosmetics, soaps, polymer additives and coatings(Aljarilla Jiménez, 2010). Rapeseed oil can be transesterified with methanol and acid to obtain a mixture of methyl esters with 16, 18 and 20 carbon atoms(Spekreijse et al., 2017). Sunflower oil, waste coffee oil and a wide range of microbial oils serve as potential ethenolysis substrates. The presence of double bonds in fatty acid esters of sunflower, soybean, rapeseed and linseed oil has been potentially explored to obtain terminal alkenes through ethenolysis and to form functionalized polymeric products subsequently. The present work explored utilization of used cooking oil, lipids from spent hen and canola oil that are elaborately discussed in Chapter 2.

1.4.1 Limiting factors to ethenolysis and ways to enhance the performance

1.4.1.1 Isomerization/Double Bond migration

Isomerization of olefins during ethenolysis of fatty esters reduces yield (formation of side products) and limits industrial application. Grubbs found that electron deficient benzoquinone can be used as additive to suppress isomerization of allylic ethers and long-chain aliphatic alkenes during olefin metathesis reactions with ruthenium catalysts as highlighted in Scheme 1.3(Dragutan et al., 2010).
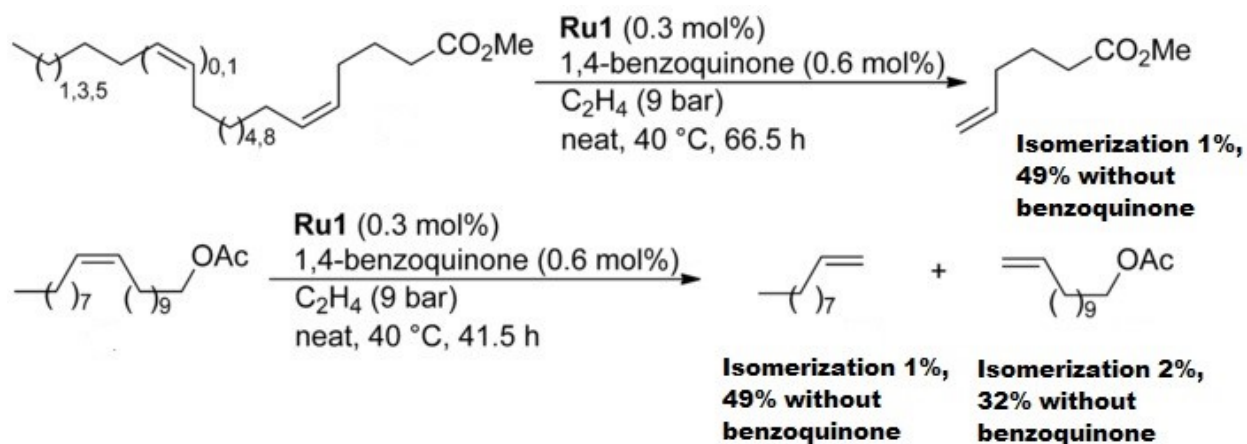
Scheme 1.3: Contribution of benzoquinone in suppressing isomerization during ethenolysis of methyl ester {Adapted with permission from Alkene Metathesis and Renewable Materials: Selective Transformations of Plant Oils. Copyright © 2008, Springer Science 2010 (Dragutan et al., 2010)}(Spekreijse et al., 2017)(Spekreijse et al., 2017)(Spekreijse et al., 2017)(Spekreijse et al., 2017)(Spekreijse et al., 2017)(Spekreijse et al., 2017)

1.4.1.2 Heating route and temperature

Catalyst used in ethenolysis reaction such as ruthenium-based catalyst decomposes quickly at higher temperature. The conventional heating can be replaced with sustainable physical techniques

such as microwave (oscillating reorientation of dipoles, heat generated by friction and dielectric loss) and ultrasound (acoustic cavitation; bubbles formation, expansion and collapse thereby releasing energy). Rapid microwave irradiation can diminish catalyst decay by quickly and homogeneously reaching the high temperature required for metathesis reaction. On the other hand, ultrasound technique can be utilized as a benign method for metathesis reaction as well as chemical reactions involving water insoluble catalyst as highlighted in Figure 1.5(Dragutan et al., 2010).

Most of the ethenolysis reaction is carried at lower temperature which improves the selectivity but diminishes the high reactivity of the catalyst. Also, stability of the incorporated catalyst is highly dependent on reaction conditions. For example, half-lives at 55°C for triisopropylphosphine methylidene $[RuCl_2(PiPr_3)_2(=CH_2)]$(Ulman & Grubbs, 1999) and pyridine based methylidene complex$[RuCl_2(PCy_3)(H_2IMes)(=CH_2)]$(Hong et al., 2007) were found to be 8 min and 340 min respectively, indicating that subtle modifications can strongly affect the stability of the metathesis intermediates. Thus, temperature must be optimized for the reactions to achieve maximum lifetime and efficiency of the catalyst.

For the ethenolysis of viscous compounds, such as methyl ricinoleate (obtained by transesterification of ricinoleic acid from castor oil seeds), a higher temperature was required to reduce the viscosity and improve the ethylene solubility. For this reason, the optimal temperature for methyl ricinoleate ethenolysis was found to be 80°C. Suitable catalyst must be incorporated to achieve better performance at this temperature. Similarly, for the ethenolysis of polymeric materials, a higher temperature may be needed to dissolve the polymer. For example, the branched copolymer of ethylene, 1-octene and butadiene fully dissolves in toluene at 70°C(Spekreijse et al., 2017).
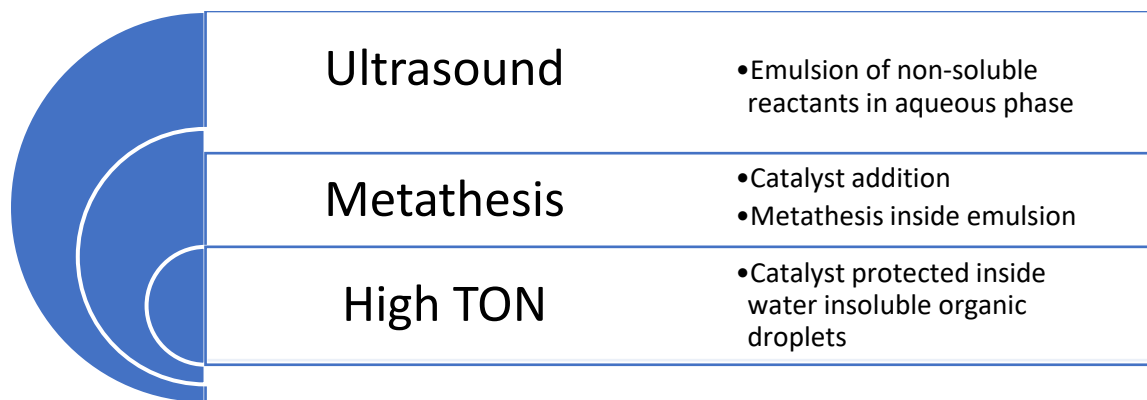
Figure 1.5: Greener and efficient route for metathesis reaction using water insoluble catalyst

1.4.1.3 Quality of biomass derived feedstock

It is important to mention that the quality of biomass derived feedstock plays an important role in the ethenolysis reaction. Feedstock may contain impurities which can act as catalyst poison thus deteriorating the efficacy of the system. It is reported that thermal treatment or purification over active supports such as alumina or magnesol can prevent the decomposition of the catalyst(Bidange et al., 2016). The amount of peroxides (which act as catalyst poison) in the feedstock can be drastically reduced with thermal treatment (Al_2O_3, 200°C) and it can significantly contribute to increase in TON.

1.4.1.4 Solvent

Self-metathesis reactions can be prevented by adding a suitable solvent. This can suppress formation of side products or unwanted products in the ethenolysis reaction. It is reported that when toluene is used as a solvent, the self-metathesis reaction is successfully suppressed and both first generation catalysts, bearing phosphine ligands, and second-generation catalysts, bearing NHC (N-heterocyclic carbene) ligands, yield full selective ethenolysis reactions(Thurier et al., 2008). Common solvents for metathesis reactions, dichloromethane and aromatic solvents, such

as toluene, are harmful to the environment and toxic. For this reason, ethenolysis reaction has been explored in dimethyl carbonate. The literature mentions that similar conversions were reached for toluene (88%) and dimethyl carbonate (82%) using 2.5 mole% (25000 ppm) ruthenium-based catalyst at room temperature for 3 h and 1 bar ethylene.

1.4.1.5 Pressure

Increasing the pressure of gaseous reactant can either increase the selectivity as reported in the case of ethyl oleate ethenolysis or it can reduce selectivity as reported during ethenolysis of oleonitrile Carbon dioxide can also be added to the ethenolysis reaction for increased reactivity, and pressure becomes a crucial factor in this system. When the pressure is increased to 120 bar, the reaction is slowed down significantly(Spekreijse et al., 2017). Optimization of these factors are required to achieve the best performance and a high process efficiency.

1.5 Polyester: A versatile polymer

Polyesters have been widely used to produce synthetic fibers, films, beverage bottles, and molded plastic parts, because of its good physical characteristics and superior thermomechanical properties. It must be highlighted that the properties of these polyesters, such as melting point, crystallinity, mechanical strength, as well as biodegradability, greatly depend on the chemical structure and the molecular weight of the polyester. For example, the polyesters produced from butanediol and succinic acid possess a high melting point(Zhu et al., 2003). The linear polyesters have different physical properties depending on their chemical structures, symmetries, and conformational features. One of the important properties of polyesters is their low gas permeability. Loss of CO_2 from carbonated beverage packages and O_2 ingress from the atmosphere into packages containing oxygen-sensitive products can limit shelf life, so improved gas barrier properties can increase package performance. Their glass transition temperatures (Tg), a property

of the amorphous phase, fall steadily with increasing alkylene group length. PET film is widely used as a packaging material for food, pharmaceuticals, electronics and medical products, because of its good mechanical properties and low cost. However, there is a continuing practical need to improve barrier properties of PET.

1.5.1 Conventional method of polyester synthesis

Polyester is typically manufactured by step-growth polymerization in a two-step reaction. The first step involves transesterification of dimethyl ester with diol to form an intermediate diester and oligomers, followed by subsequent condensation reaction in the second step to form the polymer. Other route of manufacturing PET involves direct esterification of the diacid with the diol, along with the polycondensation reaction. Generally, catalysts are not used for this reaction, since the acid functional groups of TPA can catalyse the reaction. Water formed during the reaction as a by-product should be collected for the estimation of the reaction conversion. In the commercial reaction, some PET prepolymer (BHET) is added in order to shorten the reaction time. The overall reaction time, including the esterification and the polycondensation processes, is long and usually varies from 5 to 10 h (Chegolya et al., 1979). During polymerization, small molecule by-products like diol are produced, so that high vacuum system is required to eliminate the by-product. Usually during the polymerization reaction there are some side reactions, including thermal degradation, hydrolysis, cyclization, and diethylene glycol (DEG) formation. These side reactions have a remarkable influence on the physical properties of the polymeric product. A phosphorous-based stabilizer is commonly added with the catalysts to prevent color-forming degradation reactions during the polycondensation process and subsequent polymer processing. Trimethylphosphate (TMP), triethylphosphate (TEP), triphenylphosphate (TPP), and phosphoric acid (H_3PO_4) are widely used as thermal stabilizers. Gumther et al. reported small amounts of triphenyl phosphate

(a widely used thermal stabilizer) did not influence the molecular weight, but amounts larger than 0.04 mol% caused a decrease in molecular weight(Gümther & Zachmann, 1983)

1.5.2 Choice of catalyst

Germanium oxide is a potential catalyst that can be utilized for polyester production. Although it is a more active catalyst than traditionally used antimony oxide, its high cost precludes common use for commercial PET production(MacDonald, 2002). Titanium-based catalysts are more active than other metallic catalysts, they possess the disadvantage of imparting a yellow colour to the polymer(Gandini et al., 2009). Titanium based catalysts are prone to hydrolysis to form oxoalkoxides, which have reduced activity and make the polymer hazy. Therefore, conventional antimony-based catalyst was investigated in this research which is elaborately discussed in Chapter 3. In the presence of excess catalyst, the intrinsic viscosity of the resultant PET falls, because there is a competition for catalyst between the sites responsible for the polymerization reaction like chain end groups and internal sites on the formed polymer, like ester oxygens(Shah et al., 1984). Therefore, the amount of catalyst incorporated in this work was less than <0.02% (to the amount of feedstock).

1.5.3 Challenges associated with fossil-based PET

Most plastics commercially available are still derived from non-renewable (petrochemical) sources. PET or poly(ethylene terephthalate) were manufactured as industrial products by ICI (UK, 1949) and DuPont (USA, 1953) soon after the technology of manufacturing was developed by Whinfield and Dickson in 1946. This is traditionally being produced from ethylene glycol (EG) and terephthalic acid (TPA) or dimethyl terephthalate (DMT). Ethylene glycol, a common antifreeze, coolant and industrial solvent, is responsible for many instances of accidental and intentional poisoning annually. Following ingestion, EG is first hepatically metabolised to

glycoaldehyde by alcohol dehydrogenase. Glycoaldehyde is then oxidised to glycolic acid, glyoxylic acid and finally oxalic acid. While ethylene glycol itself causes intoxication, the accumulation of toxic metabolites is responsible for the potentially fatal acidosis and renal failure, which characterises ethylene glycol poisoning(Brent, 2001). Apart from the inherent toxicity of used components, there has been a rising concerns of the environmental impact of these plastics and their dependency on (depleting) fossil reserves. These challenges have triggered the search for more sustainable alternatives in the 21st century.

Recently, green EG has been produced from renewable resources that allow certain polyesters to be partially (e.g.PET) or even fully (e.g.PEF) bio based. Looking at the scale of yearly PET consumption (estimated at 100 million tons in 2016), the use of green EG would result in non-negligible contributions to its sustainability, as PET is only partially (±30%) bio based. Such a strategy is already being employed by the Coca Cola Company for its Plant Bottle packaging (30% bio-based PET). Currently, bio-EG is primarily produced from fermentative bio-ethanol, which is dehydrated to ethylene and converted to EG according to the conventional petrochemical process. However, the main disadvantages of this process are (i) the high cost of ethanol feedstock compared to fossil ethylene,(ii) its multi-step nature (by de- and re-functionalizing, thus not using the initial functionalities of the intrinsic biomass) and(iii) its dependency on edible carbohydrate feedstocks(De Clercq et al., 2017). To overcome these challenges, it is imperative to use affordable and renewable feedstock from non-edible sources and judiciously producing it with minimum steps involved during their processing.

The sustainable character of bio-based plastics is generally embraced by scientific community and preferentially exploited by industrialists for economic advantage. Aliphatic dicarboxylic acids (ADA) that can be obtained from carbohydrates by the lignocellulosic feedstock biorefinery,

including succinic acid, fumaric acid and itaconic acid, are very important monomers. Also, examples of carbohydrate-based aliphatic diols include isosorbide, isomannide and isoidide, 1,3-propanediol and 1,4-butanediol. Suberin and cutin are two other interesting sources of monomers for the preparation of biodegradable polymers. Referring to aromatic monomers, carbohydrates and lignin are the major sources, with 2,5-furandicarboxylic acid (FDCA) and vanillic acid being the most important examples(Papageorgiou et al., 2014). Fully bio-based alternatives such as polylactic acid (PLA)or polybutylene succinate (PBS) only constitute minor fractions of the total amount of bioplastics.

However, a product's sustainability is not only determined by its origin (e.g. oil or biomass) or production process, but also by its end-of-life applications. The main conventional methods to deal with polymer wastes include landfilling, incineration, mechanical recycling and, to a lesser extent, thermal depolymerization (cracking) of polymers back to crude oil-like product mixtures. Treating bioplastics in the same way would result in the loss of opportunity to further reduce raw material demands and environmental impacts. Instead, a circular economy approach, wherein polymers can be chemically recycled (e.g.by depolymerization) or repurposed for other application would be more durable. This implies a pivotal role for bio-based polyesters, since ester linkages are susceptible to controlled depolymerization (e.g.by solvolysis)(De Clercq et al., 2017).

Chapter 2: Solvent-free rapid ethenolysis of fatty esters from spent hen and other lipidic feedstock with high turnover numbers

2.1 Introduction

Humanity have witnessed a tremendous technological improvement in the last century through scientific progress and evolved management practises. However, most of the advancements have been viewed through the lens of economic aspect, without giving due accountability towards environmental and social dimensions of sustainability. Recently, there has been a transition from conventional linear model (take, make, dispose) to circular model of production where reliance on virgin materials is reduced and consumption of secondary materials for holistic growth in social, environmental and economic segments is promoted [1]. Using the concept of circular economy as our guiding principle and greener sustainable production as an objective, this chapter highlights the utilization of renewable and waste lipids to develop bio-based polymer precursors and valuable chemicals through solvent-less ethenolysis process.

According to estimates, the total global production of used cooking oil is about 29 million tons per year [2]. Canada generates more than 135 million litres of used cooking oil (UCO) [3] while the volume of UCO generated each year in UK is estimated to be 250 million litres and nearly 75 million tons is claimed to be utilized for the biodiesel production [4]. The annual production of used cooking oil is gradually increasing, leading to management issues.

Spent hen is yet another novel lipidic resource with great potential to be utilized in polymer industry as examined in this report. More than 2.6 billion spent hens are produced globally and 26 million in Canada yearly which are generally dumped in landfills once their laying capacity is impeded [5]. These data represent the pool of available resources which could beneficially serve

as non-fossil-based feedstock subjected to accomplishment of economic aspect. These resources have been explored for biodiesel production, but it suffers disadvantage in economic terms with respect to fossil-based counterparts. The competitiveness against fossil-based resources can be achieved by diversifying the range of products obtained from the biomass, such as by producing high value chemicals in addition to low-value biodiesel [6]. Olefin metathesis is considered a powerful technique to transform unsaturated oleochemicals into valuable chemicals [7]. Cross-metathesis reactions with lower alkenes result in medium-chain fatty acid esters which are highly demanded raw materials for the industrial production of surfactants [8]. Utilization of ethylene in metathesis reaction(ethenolysis) generates linear α-olefins (LAOs) which are used in variety of applications such as co-monomers for polyethylene production, for the synthesis of oxo alcohols to give detergents and plasticizers, and for making poly-α-olefins used in drilling fluids and synthetic lubricants [9]. Most of the studies reported to date have used purified methyl oleate as a model substrate for metathesis [7], and reactions were carried out in the presence of organic solvents like cyclohexane [10], dichloromethane [11], toluene [12] and other solvent mixtures [8]. Others have indicated the use of CO_2 to selectively solubilize products in vapor phase by taking advantage of low solubility of reactants to increase the reaction rate and equilibrium conversion [13]. The employment of ethenolysis process to produce bio-based styrene and acrylic acid from waste biomass has been demonstrated successfully by Sperkreijse et al. [11]. Our group has previously manifested solvent-less ethenolysis of waste oil and canola oil with highest turnover numbers attained as 15,840 and 21,450 respectively [7]. To the best of our knowledge, there are no reports on the ethenolysis of CF esters.

In this study, we performed ethenolysis without the use of organic solvents making the process environmentally benign. In addition, efforts were made to achieve rapid conversions and excellent

turnover numbers for UCO and CO esters by employing ethenolysis process without extensive purification of feedstock and catalyst.

2.2 Experimental Section

2.2.1 Materials

Canola oil (99%), chicken fat (98%), used cooking oil (96.8%), Grubbs catalyst 1st generation (G1, 97%), Grubbs catalyst 2nd generation (G2, 97%), Hoveyda–Grubb catalyst 1st generation (HG1, 97%), Hoveyda–Grubbs catalyst 2nd generation (HG2, 97%), potassium hydroxide ($\geq$ 85 %), sodium chloride ($\geq$99.5 %), anhydrous sodium sulfate ($\geq$99%) and methanol ($\geq$99.8 %) were obtained from Sigma–Aldrich. Ethylene gas (Praxair Inc., 99.9 %), silica gel used for column chromatography (70–230 mesh, 60 Å pore size), flash silica (Silicycle, 40–63 mm, 230–400 mesh), thin layer aluminium chromatographic plates (Sigma-Aldrich, 0.20 mm thick, 20×20 cm size, binder polymeric, fluorescent indicator), ethyl acetate (Fisher, 99.9 %), and n-hexane (Caledon) were purchased and used as received.

2.2.2 Methods

All the reactions were performed on a customized microwave (Matthews, USA), in a 500 mL batch scale-up pressure reactor. The cylindrical vessel (15 cm outer diameter, 17 cm maximum height and 2 cm wall thickness) was made from PEEK material with the operating limits of 250°C and 100 psi. The reactors were purged with N_2 prior to transfer of methyl esters. The quantity of methyl esters varied between 100-150 g and corresponding amount of catalyst was calculated to maintain its' concentration between 5-50 ppm. Catalyst was transferred to the reaction vessel inside the glove box (with flow of nitrogen) to eliminate every trace of oxygen. The vessel was sealed and then placed inside the microwave system. The pressure of ethylene (60 psi) was applied and the reactions were heated (50°C) and stirred during the reaction time (30 minutes). Experimental set-

up employed for processing of various renewable and waste fatty-acid methyl esters is represented in Figure 2.1. Air stirrer ensured homogenous mixing of catalyst and feedstock, while temperature probe was used to monitor temperature changes during the reaction. Outer channels of gas pipes and temperature probe was sealed with Teflon tape to avoid any leakage of components during the ethenolysis process. After the reaction, the reactors were opened, and an aliquot was filtered over a plug of silica prior to their injection into the GC-MS. The composition of ethenolyzed products was evaluated with GC-FID analysis by calculating corresponding area at retention time of each component. These are highlighted and elaborately discussed for UCO esters, CO esters and CF esters in Table 2.2, 2.3 (a), 2.3 (b) and 2.5 at catalyst loadings between 5-50 ppm for G2 and HG2 catalysts. Moreover, the components were analysed in TLC plates (Figure 2.10, R_f values), then separated into olefins, esters and diesters fraction by column chromatography, and further examined by FTIR to validate the separation.
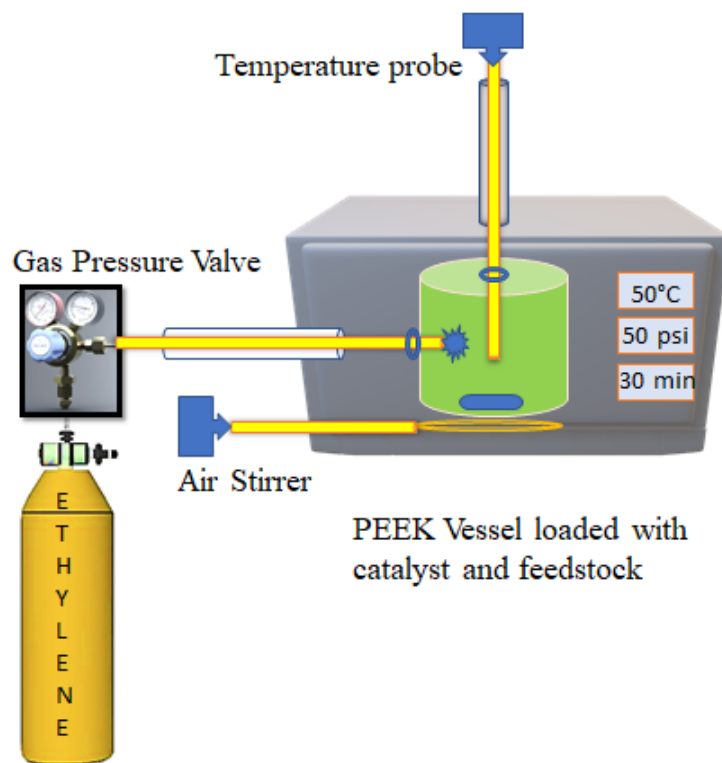
Figure 2.1: Illustration of experimental set-up for ethenolysis reaction of fatty esters

2.2.3 Characterization conditions for FTIR, GC-FID and GC-MS

ATR-FTIR spectra of the ethenolyzed components were recorded using a Bruker Optics (Esslingen, Germany) unit equipped with a single bounce diamond ATR crystal. All samples were scanned in the wavelength range of 400-4000 cm^{-1}. Spectra were obtained using OPUS software version 6.5 from Bruker and a total of 16 scans at a resolution of 4 cm^{-1} were recorded for each sample. Background scans (16 scans) were also performed manually before each fraction was analysed.

GC-MS analyses of all samples were conducted on Agilent 6890N (USA) gas chromatograph fitted with a fused silica capillary column SP2560 (100 m ×0.25 mm, 0.2 μm film thickness) linked to a detector 5975B inert XL MSD. Samples (ethenolyzed products) were dissolved in DCM for the preparation of standard solutions with different concentration. A sample volume of 2 mL was injected, the injector temperature was set to 240 °C and a split mode with ratio of 20:1 was used. The temperature profile was held at 45 °C for 4 min; then increased to 175 °C (13 °C min^{-1}) and held for 27 min; and further ramped at 4 °C min^{-1} to 215 °C and held for 35 minutes. Helium gas was used as mobile phase with a constant flow rate of 1.3 mL min^{-1}.

GC-FID analyses were conducted on PerkinElmer GC-FID Clarus 500 instrument (USA) equipped with flame ionization detector. The temperature was set at 280 °C for the detector and 240 °C for the injector. Air and hydrogen were used as carrier gases with flow rates of 450 and 45 mL min^{-1}, respectively. The column used and all other conditions were as mentioned above for GC-MS instrument Agilent 6890N. Samples (ethenolyzed products) were dissolved in DCM for the preparation of standard solutions with different concentration. Values of their peak areas were used for plotting standard curves and mass response factors were calculated. The concentrations of

corresponding FAMEs and diester in self-metathesis product are calculated using their mass response factors.

2.2.4 Grinding of Spent Hen and lipid extraction

The spent hen bought from Kasoa Tropical Food Market, South Edmonton was chopped into smaller pieces and bones were removed manually in the laboratory. The small pieces were subjected to grinding in the laboratory scale grinder (Cuisinart electric meat grinder, Model MG-100 C, heavy-duty 300 W motor). No water was added during the grinding process. The grinded sample was collected in Ziploc bags and refrigerated at -15°C until further use.

A sample of about 2000 g whole ground spent hen was placed in the 12 L chemglass 3-neck round bottom reaction vessel (Figure 2.2) with a solvent-to-feed ratio of 1.3 mL/g of dichloromethane-methanol (2:1, v:v) on a wet basis. The mixture was agitated by using heidolph RZR1 overhead stirrer with stirring speed maintained manually between 280-500 rpm. The extracted portion was collected through the manual opening provided at the bottom of the vessel. The collected sample was separated into two layers of water and solvent component. The lipidic portion in solvent layer was recovered by evaporating the solvent using rotary evaporator under vacuum at 35 °C as shown in Figure 2.2. The lipidic part was passed through the sodium sulphate to remove remaining traces of moisture before transesterification.

A   B   C

Figure 2.2: (A) Chemglass 12L 3 neck falsk for lipid extraction

(B) Separating solvent layer(bottom) and aqueous layer(top) obtained from extracted portions

(C) Removal of moisture traces from oil by passing it through sodium sulphate

2.2.4 General procedure for microwave assisted ethenolysis

Fatty acid methyl esters were prepared by direct transesterification of triglycerides of CO, UCO and CF according to the previously reported method [14]. In the pre-treatment process, prepared esters were passed through flash column of silica, alumina and anhydrous sodium sulphate to remove color pigments, impurities and moisture. Desired mass of reactants was taken in 500 ml PEEK closed vessel and purged with N_2 and ethylene gas. Measured quantity of catalysts was transferred into the reaction vessel in an inert environment nitrogen gas (inside glove box).

The ethylene pressure in the reactor was adjusted to 60 psi, where the reaction mixture was stirred and heated to 50 °C for 30 minutes. After completion of the reaction, the reactor was cooled down to room temperature and the reaction contents were filtered over a short plug of silica prior to their characterization with GC-FID and GC-MS.

2.3 Results and Discussion

2.3.1 Catalyst Screening

A screening of several commercially available catalysts (as shown in Figure 2.3) was performed on esters of CO, CF and UCO for their ethenolysis using 50 ppm concentration of catalyst for reaction condition maintained at 60 psi (ethylene) and 50°C. Both the phosphine based first generation catalysts (G1 and HG1) showed little or no conversion, while NHC (N-Heterocyclic Carbene) ligand based HG2 and G2 proved to be active catalysts for CF and CO, UCO substrates. The ethenolysis of CO and CF substrate provided high conversions and TONs with HG2 catalyst while in case of UCO esters, G2 catalysts was the one among four catalysts (Figure 2.3) which displayed higher conversion rate and TONs. This disparity suggests that the reactivity of Grubbs and Hoveyda-Grubbs catalyst is significantly affected by the fingerprint of the participating reactant moieties (varying degree of unsaturation of various lipidic sources and presence of other inactive components). Similar study of substrate dependent kinetics was showcased earlier by Vincent et al. [15]. As the quality of biomass derived feedstock affects the reactivity and efficacy of catalysts, effort is required to identify suitable catalyst-feedstock system. These are investigated elaborately in terms of conversion, yield, turnover numbers (TONs) and turnover frequency (TOF). Turnover numbers were tuned by adjusting the amount of catalyst loading.
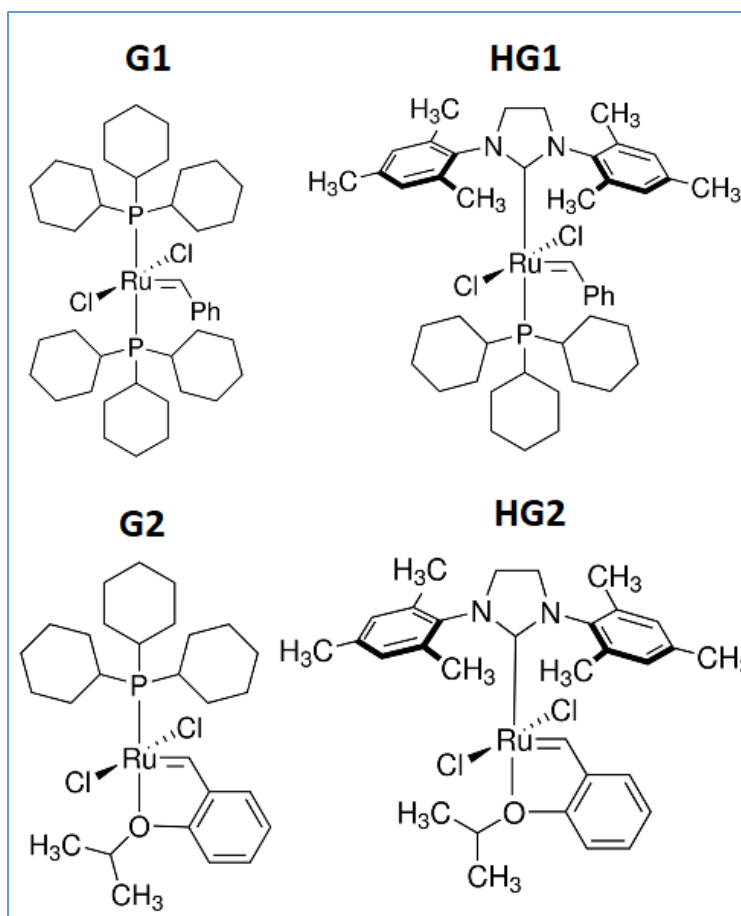
Figure 2.3: Catalysts used for solvent-less ethenolysis of lipids to obtain polymer precursors

2.3.2 Turnover Numbers (TONs)

Maximum turnover numbers obtained for CO, UCO and CF esters were 92000, 78080 and 21820 at low catalyst loading of 10 ppm, 7.5 ppm and 20 ppm respectively as shown in Table 2.1. Further decreasing the catalyst loading resulted in decrease of TONs (see Table 2.5, Table 2.6, Table 2.7), that hold less or no commercial significance. For economic viability, metathesis turnover numbers greater than 50,000 are desirable for homogeneous catalysis [16]. The present study suggests that HG2 catalysts exhibited excellent TONs only at higher catalyst loading, and perhaps becomes susceptible to decomposition at catalyst loading less than 20 and 10 ppm for ethenolysis of CF esters and CO esters respectively. On the other hand, G2 catalyst manifested lower catalytic rate

than HG2 thereby generating less TONs for CF esters and CO esters (see Table 2.6 and Table 2.7). However, the presence of saturated lipid moieties and several other non-triglyceride components in UCO esters (see Table 2.8) have pronounced effect on the decomposition of HG2 catalysts. Consequently, maximum TONs for UCO ester were achieved with 7.5 ppm G2 catalysts enumerated as 78080.

Table 2.1: Highest Turnover numbers achieved by ethenolysis of CF, UCO and CO methyl esters

Feed	Catalyst	Loading (mol%)	T (°C)	Hold Time (min)	Conv. (%)	Yield (%)	TON[a]
CF ester	HG2	0.00200	50	30	53	45.0	21820
UCO ester	G2	0.00075	50	30	59	45.7	78080
CO ester	HG2	0.00100	50	30	93	71.0	92000

2.3.3 Scheme for ethenolysis

The schematic diagram for ethenolyzed products from esters of canola oil, used cooking oil and chicken fat is depicted in Scheme1. The additions of catalysts to esterified feedstocks lead to the formation of numerous terminal olefins, internal olefins and unsaturated monoesters. The compositions for feedstocks are elaborately mentioned in the supporting document (see Table 2.8). The characterization of various CF esters components (reactants) and ethenolyzed products were performed using GC-MS. The identification of individual constituents was governed using retention time characteristics. As shown in Figure 2.4, the signal marked as A, B, and C corresponds to saturated components [palmitic acid methyl esters($C_{17}H_{34}O_2$), stearic acid methyl esters($C_{19}H_{38}O_2$) and myristic acid methyl esters($C_{15}H_{30}O_2$)] which are inactive towards metathesis reaction. Peak with a retention time of 33.9 min represents R1 [oleic acid methyl esters

(C$_{19}$H$_{36}$O$_2$)] and its intensity is reduced in the product spectra as manifested in Figure 2. Likewise, R2 [linoleic acid methyl esters(C$_{19}$H$_{34}$O$_2$)], R3 [linolenic acid methyl esters(C$_{19}$H$_{32}$O$_2$)] and R4 [palmitoleic acid methyl esters (C$_{17}$H$_{32}$O$_2$)] displayed decrease in peak intensity, indicating consumption of reactant components during the ethenolysis process.
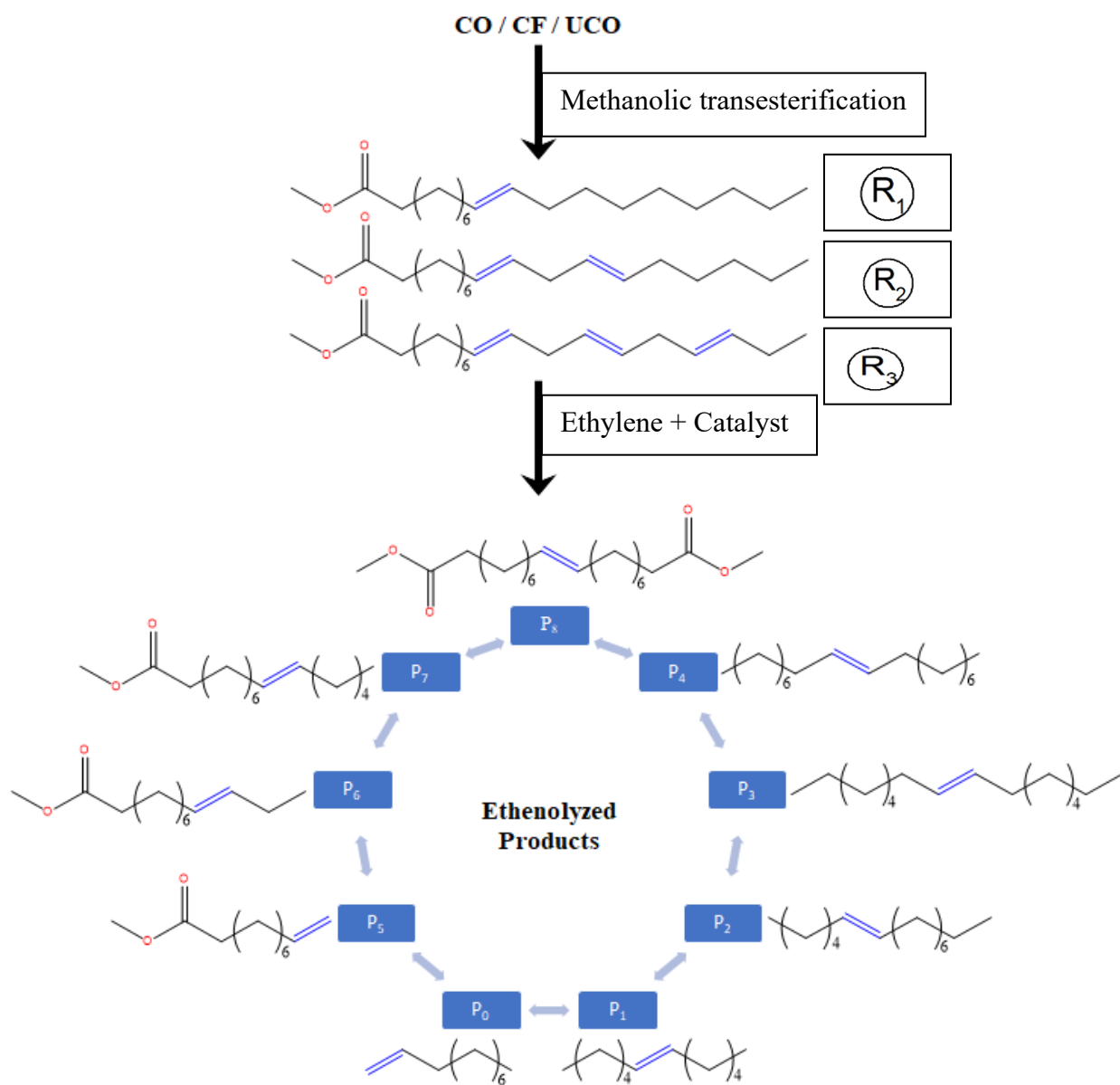
Scheme 2.1: Ethenolyzed and self-metathesized products obtained from esters of CO, CF and UCO

2.3.4 GC-FID analysis for ethenolyzed product from Used Cooking Oil (UCO)

Table 2.2: Area obtained for corresponding components after ethenolysis of UCO esters with G2 catalysts, acquired by GC-FID analysis

Components Cn:m	50 ppm	20 ppm	10 ppm	7.5 ppm	5 ppm
	Area at different catalyst loading(G2) after ethenolysis				
C10:1 H	897.05	469.11	407.70	191.5	-
C12:1 H	572.2	406.55	354.87	203.76	216.09
C15:1 H	1530.72	1161.95	1155.90	1340.21	539.48
C16:1 H	236.9	451.08	428.59	385.68	375.5
C18:1 H	1359.34	1243.51	776.70	679.88	530.19
C10:1 ester	1089.66	1079	538.07	384.42	398.02
C12:1 ester	485.53	346.84	375.57	115.67	149.78
C15:1 ester	2159.96	2223.77	1970.94	1117.88	1207.86
C18:1 ester*	3755.74	4073.24	2660.12	2278.81	1426.77
C18:2 ester*	2325.66	5142.1	4941.50	3238.43	3043.74
Diester	4172.2	3419.23	1990.03	2006.62	1681.77

Components marked with * denotes isomerised products

Area highlighted in Table 2.2 calculated by GC-FID, represents quantity of corresponding components (ethenolyzed products) obtained by ethenolysis of UCO esters at various catalyst loadings of G2 catalyst. "Cn:m H" corresponds to olefins, where n denotes carbon chain length and m denotes number of double bonds. Similarly, "Cn:m ester" represent esters where m=1 signify monoester components and m=2 signify diesters. It is inferred here that lowering the

catalyst loading resulted towards gradual decline in conversion and yield (olefins, monoesters, diesters) whereas incongruous and non-linear trend was observed during the formation of isomerised products. Exceptionally high amounts of isomerised products were formed at 20 ppm which decreased with further reduction of catalyst amount.
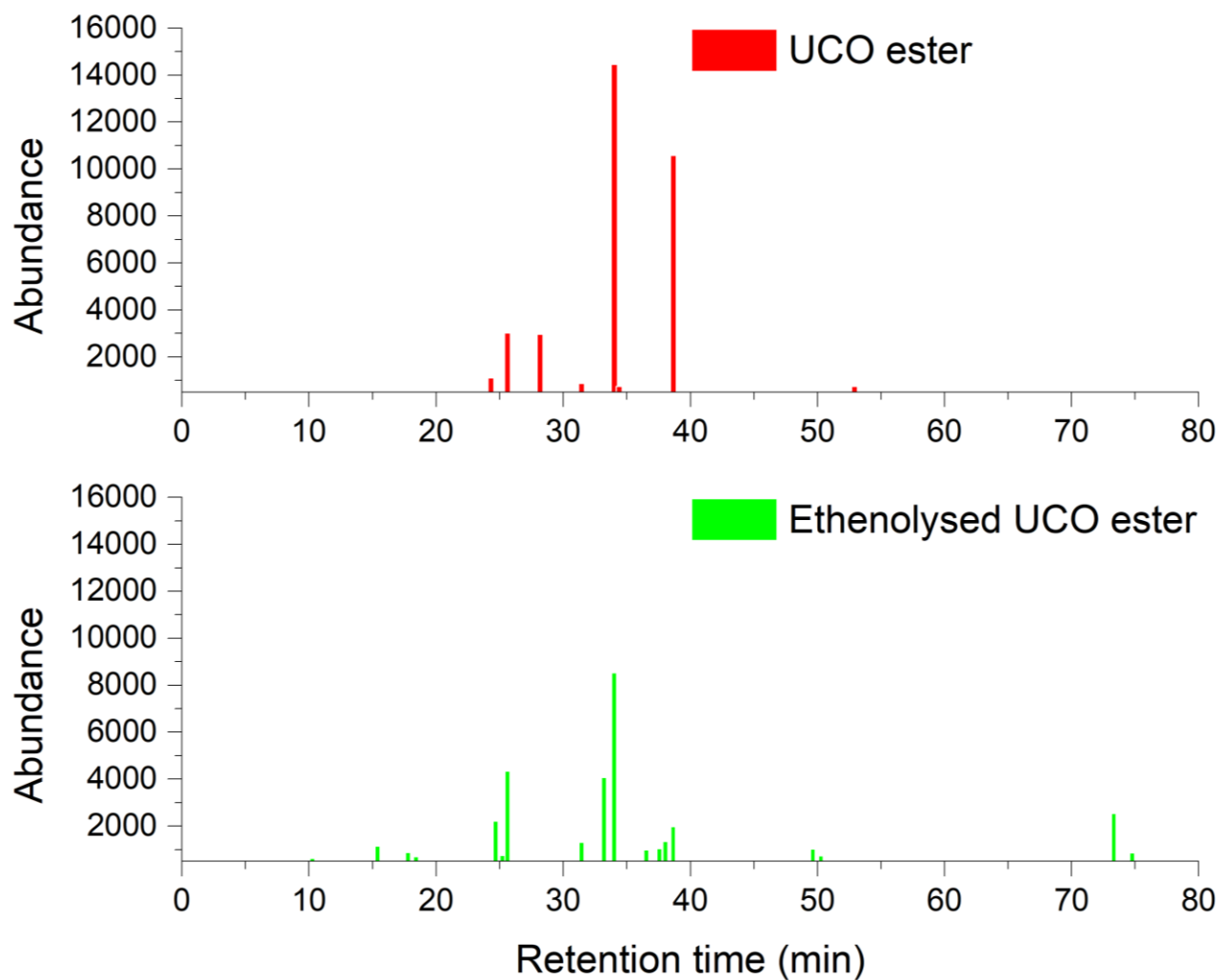
Figure 2.4: GC-FID spectra of UCO esters and its ethenolyzed products with 50 ppm G2 catalyst

2.3.5 GC-FID analysis for ethenolyzed product from Canola Oil (CO)

Table 2.3 (a): Area obtained for corresponding components after ethenolysis of CO esters with HG2 catalysts, acquired by GC-FID analysis

Components	50 ppm	20 ppm	15 ppm	10 ppm
	Area at different catalyst loading (HG2) after ethenolysis			
C10:1 H	3669.8	1934.1213	3527.01	1385.88
C12:1 H	712.86	385.6548	480.93	708.11
C15:1 H	1605.18	1223.9636	1400.24	1700.75
C16:1 H	380.21	314.2501	362.62	503.89
C18:1 H	2726.86	2425.1076	2828.87	2660.99
C10:1 ester	1812.94	769.6097	1198.76	957.42
C12:1 ester	1293.41	842.2693	1112.13	1360.26
C15:1 ester	2563.66	1986.4266	2192.3	2557.02
C18:1 ester*	6543.04	5601.6155	6825.69	6648.32
C18:2 ester*	3024.08	2434.9866	3118.02	6178.23
Diester	6063.81	3722.7454	5316.30	1681.77

Components marked with * denotes isomerised products

Area highlighted in Table 2.3 (a) calculated by GC-FID, represents quantity of corresponding components (ethenolyzed products) obtained by ethenolysis of CO esters at various loadings of HG2 catalyst. A high amount of dec-1-ene (C10:1 H) was observed with catalyst loading of 15 ppm, demonstrating optimized feedstock/catalyst ratio and signifying greater affinity towards cross-metathesis with ethylene. There was no significant change in the amount of isomerised product of oleic acid methyl esters($C_{19}H_{36}O_2$) formed at different catalyst loadings. An abrupt

change in the amount of isomerised linoleic acid methyl esters ($C_{19}H_{34}O_2$) was observed at 10 ppm of catalyst loading. A considerable quantity of isomerised products was obtained at the expense of formation of terminal olefins and diesters.

Table 2.3 (b): Area obtained for corresponding components after ethenolysis of CO esters with G2 catalyst, acquired by GC-FID analysis

Components Cn:m	20 ppm	15 ppm	10 ppm	7.5 ppm	5 ppm
	Area at different catalyst loading(G2) after ethenolysis				
C10:1 H	1324.3	1790.46	1645.07	-	-
C12:1 H	294.66	300.47	261.06	200.04	-
C15:1 H	902.8	675.09	943.84	1087.87	379.7
C16:1 H	153.52	235.01	150.78	208.79	331.73
C18:1 H	1845.11	1176.61	1476.94	1396.97	352.23
C10:1 ester	1052.26	345.78	445.14	821.24	193.3
C12:1 ester	624.37	633.85	1260.44	399.25	245.5
C15:1 ester	1428.57	705.20	1051.82	1389.47	410.68
C16:1 ester	405.51	715.18	786.77	594.48	129.13
C18:1 ester*	4125.49	3041.70	3715.59	3568.49	895.11
Diester	3562.03	2245.45	3097.06	3304.92	957.07

Components marked with * denotes isomerized products

Area highlighted in Table 2.3 (b) calculated by GC-FID, represents quantity of corresponding components (ethenolyzed products) obtained by ethenolysis of CO esters at various loadings of G2 catalyst. Notably high amount of dec-1-ene (C10:1 H) was observed at 15 ppm catalyst loading, thereby exhibiting identical result as underlined with HG2 catalyst in the previous section. Lower conversion was obtained, and insubstantial quantities of components were formed at 5 ppm

catalyst loading. No significant change was observed in the amount of isomerised product formed at various other catalyst loadings.

Table 2.4 (a): Ethenolysis of renewable canola oil derived methyl esters

Entry	Catalyst	Loading [ppm]	Temperature [°C]	Hold time [min.]	*Conv. [%]	*Yield [%]	*TONs
1	HG2	50	50	30	96	83.5	21710
2	HG2	20	50	30	94	62.6	40710
3	HG2	15	50	30	95	83.8	72630
4	HG2	10	50	30	93	71.0	92000
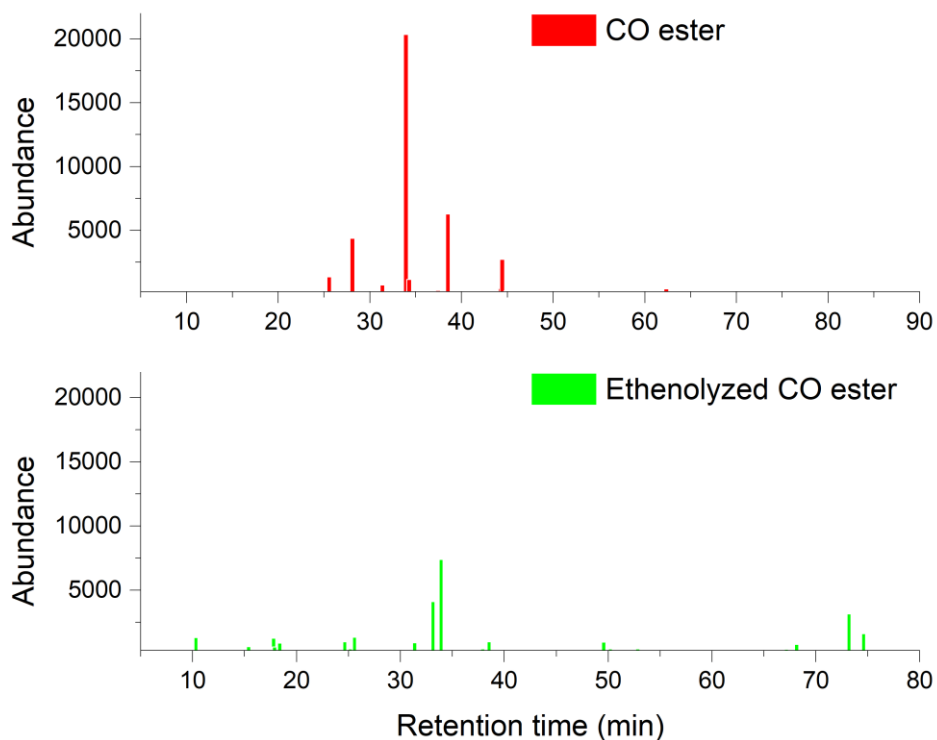
Figure 2.5: GC-FID spectra of CO esters and its ethenolyzed products with 50 ppm HG2 catalyst

The selection of catalyst to perform ethenolysis of CO esters was made by assessing four different catalysts (G1, G2, HG1 and HG2) at 60 psi and 50°C. The most favourable catalyst (second-generation Hoveyda Grubbs catalyst) was deployed at different loading to evaluate conversion, yield and TONs for ethenolysis of CO esters as shown in Table 2.4(a). In this study, catalyst at 50 ppm loading exhibited the highest conversion and yield (96% and 83.5% respectively). Lowering the catalyst amount had no significant effect on conversion percentage but yield percentage was influenced with change in catalyst loading. Highest TONs of 92000 were obtained with 10 ppm catalyst loading which exhibited 93% conversion and 71% yield. Additionally, the conversion and yield obtained at catalyst loading of 15 ppm was 95% and 83.8% respectively with TONs enumerated as 72630. At 20 ppm, the conversion was maintained at 95% with 83.8% yield and TONs were calculated as 40710.

Table 2.4 (b): Ethenolysis of renewable canola oil derived methyl esters

Entry	Catalyst	Loading [ppm]	Temperature [°C]	Hold time [min.]	*Conv. [%]	*Yield [%]	*TONs
1	G2	20	50	30	67.6	67.4	44170
2	G2	15	50	30	62.5	51.8	45270
3	G2	10	50	30	68.8	59.4	77800
4	G2	7.5	50	30	68.3	48.2	84190
5	G2	5	50	30	18.7	12.9	35290

Table 2.4 (b) highlights conversion, yield and TONs obtained with G2 catalyst for the ethenolysis of canola oil derived esters. The highest TONs of 84190 were achieved with the catalyst loading of 7.5 ppm. This was marginally less that that obtained with HG2 catalyst. The conversion was maintained in the range of 60%-70% for varied catalyst loading up to 7.5 ppm. Further decreasing the catalyst amount significantly reduced the conversion to 18.72% with TONs enumerated as 35290. Linear pattern was not observed in terms of yield percentage with the amount of catalyst

loading. This was attributed to varied distribution of isomerised products at different catalyst loading. Maximum yield of 59.39% was achieved at 10 ppm loading of G2 catalyst.

2.3.6 GC-FID analysis for ethenolyzed product from Chicken Fat (CF)

Table 2.5: Area obtained for corresponding components after ethenolysis of CF esters with HG2 catalyst, acquired by GC-FID analysis

Components	50 ppm	20 ppm
	Area at different catalyst loading (HG2) after ethenolysis	
C10:1 H	1672.38	2237.66
C12:1 H	237.39	240.1
C15:1 H	1081.06	544.7
C16:1 H	510.36	155
C18:1 H	1841.69	507.95
C10:1 ester	1843.3	571.8
C12:1 ester	425.41	317.78
C15:1 ester	1472.71	671.28
C18:1 ester*	4455.44	1558.74
C18:2 ester*	1602.36	5381.48
Diester	2655.44	1411.38

Components marked with * denotes isomerised products

Area highlighted in Table 2.5 calculated by GC-FID, represents quantity of corresponding components (ethenolyzed products) obtained by ethenolysis of CF methyl esters at catalyst loadings of 50 ppm and 20 ppm respectively. Monoester and diester components were obtained in considerably higher amounts at 50 ppm catalyst loading as compared to 20 ppm catalyst loading.

Lowering the catalyst amount suppressed the formation of isomerised oleic acid methyl esters($C_{19}H_{36}O_2$) but extensively enhanced the formation of isomerised linoleic acid methyl esters($C_{19}H_{34}O_2$). Similarly, shorter chain alkenes (C10:1 H and C 12:1 H) were formed enormously in high amount at 20 ppm catalyst loading. Catalyst loading below 20 ppm was not effective for metathesis reaction and insignificant conversion was obtained at low concentration

Table 2.6: Ethenolysis results for renewable chicken fats derived methyl esters with HG2 and G2 catalysts

Entry	Catalyst	Loading [ppm]	Temperature [°C]	Hold time [min.]	*Conv. [%]	*Yield [%]	*TONs
1	HG2	50	50	1	82	73.1	14630
2	HG2	20	50	30	53	45.3	21820
3	G2	20	50	30	41	31.9	16730
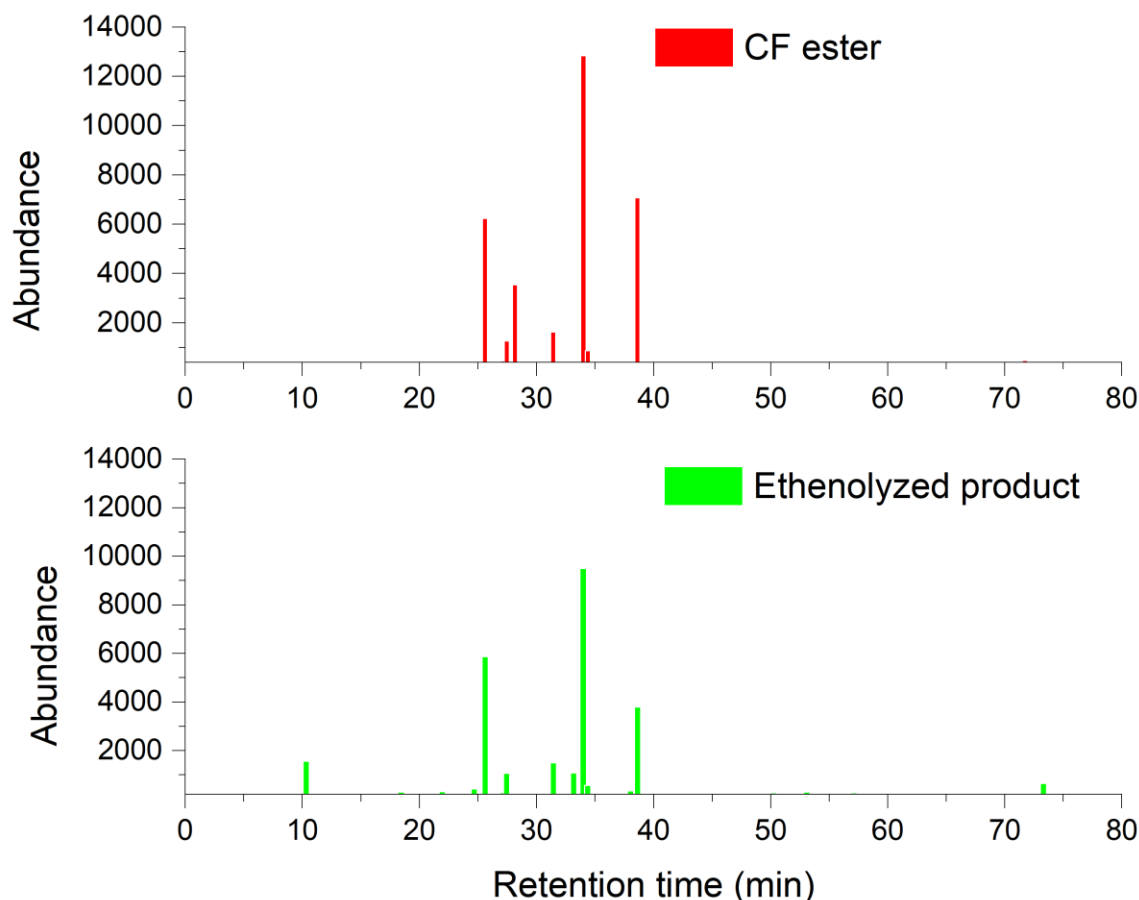
Figure 2.6: GC-FID spectra of CF esters and its ethenolyzed products with 50 ppm HG2 catalyst

The choice of catalyst for ethenolysis of CF esters was determined by evaluating for different catalysts (G1, G2, HG1, and HG2) at 60 psi and 50°C. The second-generation Hoveyda Grubbs catalyst (HG2) proved to be more proficient than other catalysts. Consequently, it was incorporated at different loading to evaluate conversion, yield and TONs for ethenolysis of CF esters as shown in Table 2.6. In this study, HG2 catalyst at 50 ppm load exhibited 82% conversion and 73.1% yield . This was significantly reduced to 53% and 45.3% respectively, at lower catalyst loading of 20 ppm. These results have shown similar trend as was observed in case of CO esters and UCO esters, while higher TONs were achieved at catalyst loading of 20 ppm. However, this was substantially

reduced on further decline in catalyst amount which was attributed to negligible conversion and poor percent yield at 10 ppm. TONs of 16730 obtained with 20 ppm of G2 catalyst was significantly lower than that obtained with HG2 catalyst and this result held lesser commercial significance. Thus, no further evaluation was undertaken at lower catalyst loading of G2.

2.3.7 GC-MS spectra for ethenolyzed product from methyl esters of Chicken Fat (CF)

The appearance of new peaks [P1-P8] in GC-MS spectrum (Figure 2.7) represents the formation of ethenolyzed products, where [P2-P4] corresponds to internal unsaturated alkenes (6-pentadecene, 8-hexadecene, and 9-octadecene) and P8 represent diesters component. Shorter chain alkenes [P0-P1] are not represented in the figure as they were eluted below the lower limit of GC column. Apart from linear olefins, several unsaturated monoesters [P5-P7] were also obtained which can be further polymerized to obtain functionalized macromolecules. Isomerised oleic acid methyl ester ($C_{19}H_{36}O_2$) [P7] was also obtained during the ethenolysis reaction. This suggests some amount of catalysts gets consumed towards isomerization of reactants, consequently leading to lower terminal alkenes and diester components. GC-MS data for other substrates (CO and UCO esters) are given in the supporting document (see Figures 2.8, 2.9).
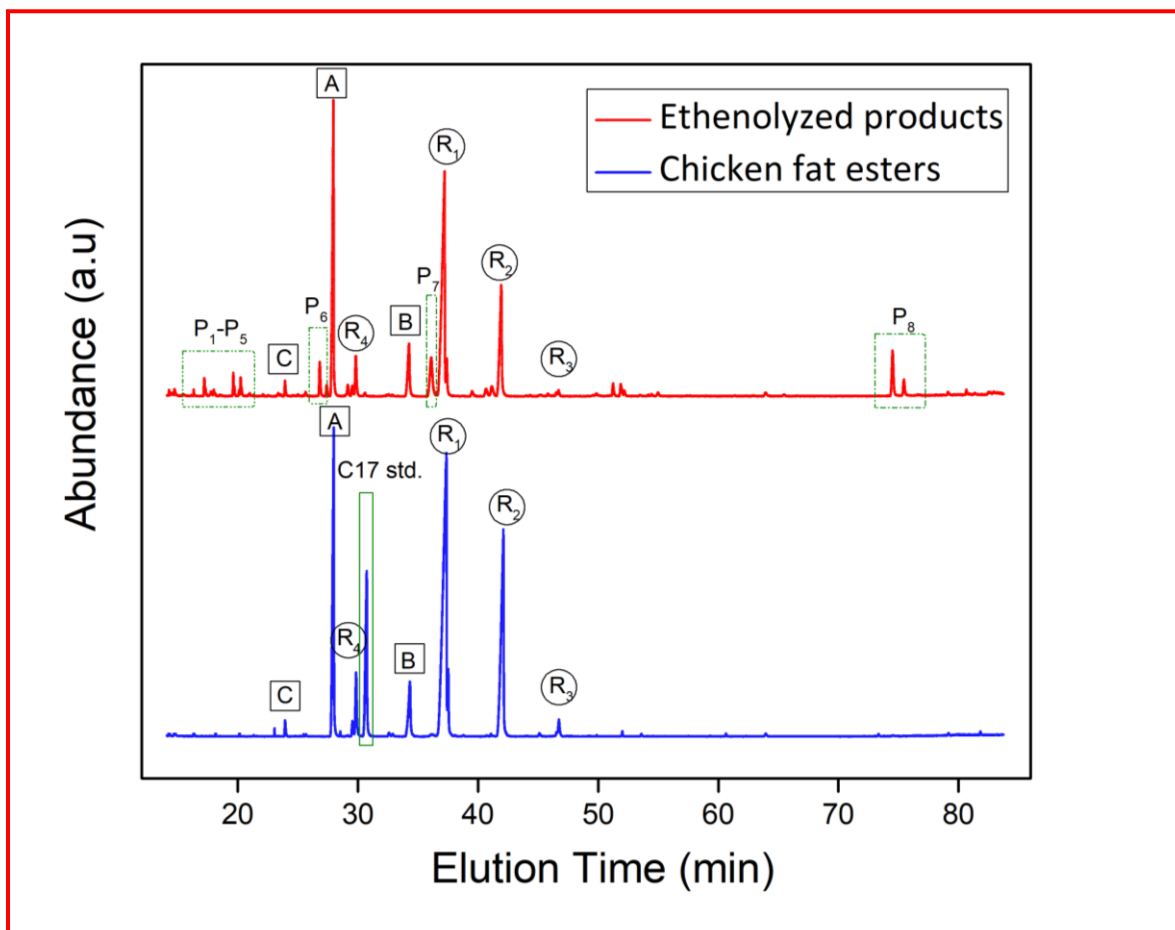
Figure 2.7: GC-MS spectra for ethenolyzed products of CF esters with 20 ppm HG-2

catalyst

2.3.7 GC-MS spectra for ethenolyzed product from methyl esters of Used Cooking Oil (UCO)
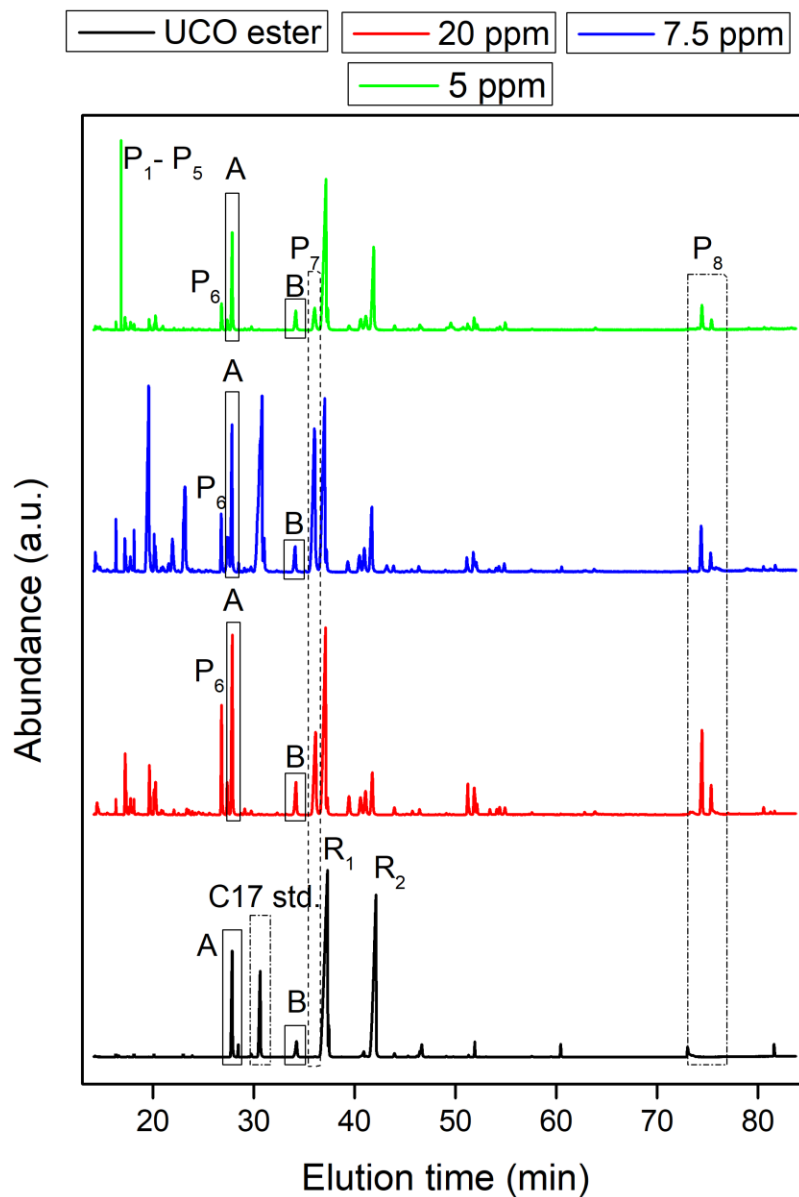
Figure 2.8: GC-MS spectra of UCO esters and its ethenolyzed products with different loading of G2 catalyst

2.3.8 GC-MS spectra for ethenolyzed product from methyl esters of Canola Oil (CO)
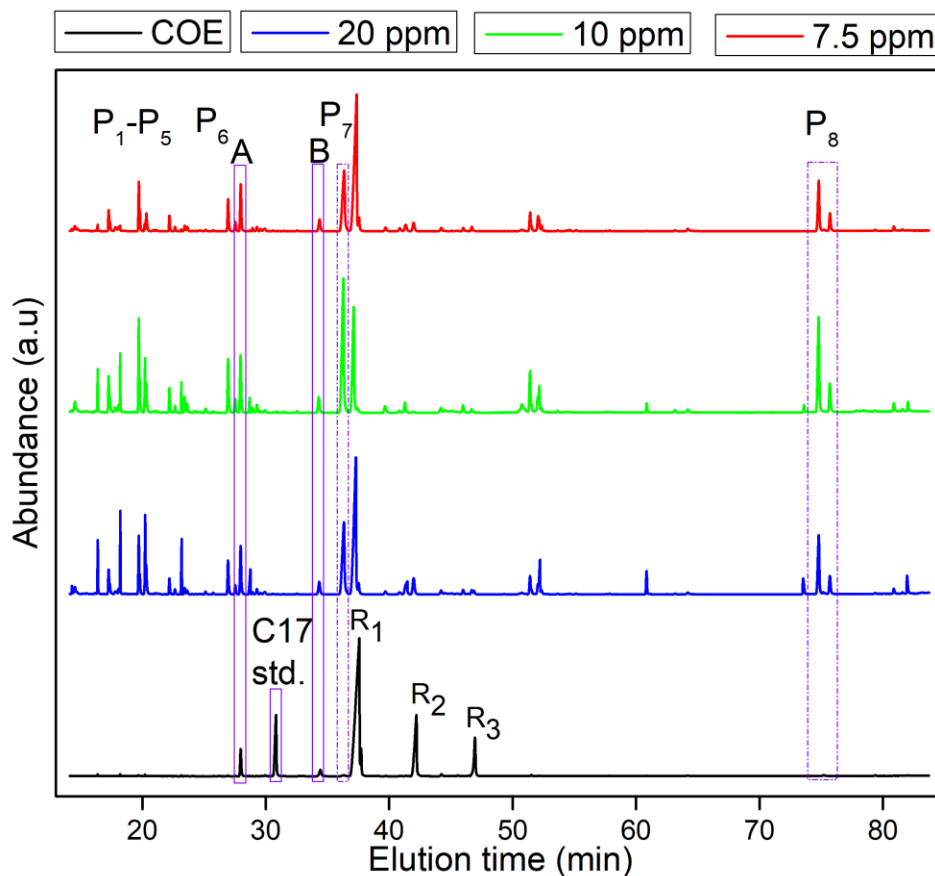
Figure 2.9: GC-MS spectra of CO esters and its ethenolyzed products with different

loading of G2 catalyst

Figure 2.8 and Figure 2.9 illustrates respectively, various components of CO and UCO esters (reactants) as well as their ethenolyzed products, identified using GC-MS. A and B corresponds to saturated components of palmitic acid methyl esters($C_{17}H_{34}O_2$) and stearic acid methyl esters($C_{19}H_{38}O_2$) which are inactive towards metathesis reaction. Peak with a retention time of 33.9 min represents R1 [oleic acid methyl esters ($C_{19}H_{36}O_2$)] and its intensity is reduced in the product spectra as manifested in Figure 2.8 and 2.9. Likewise, R2 [linoleic acid methyl esters

(C$_{19}$H$_{34}$O$_2$)] and R3 [linolenic acid methyl esters (C$_{19}$H$_{32}$O$_2$)] displayed decrease in peak intensity, indicating consumption of reactant components during the ethenolysis process.

The appearance of new peaks [P1-P8] in GC-MS spectrum (Figure 2.8 and Figure 2.9) represents the formation of ethenolyzed products, where [P1-P3] corresponds to terminal alkenes (1-pentadecene, 1-hexadecene, and 1-octadecene) and P8 represents diesters component. Shorter chain alkenes are not represented in the figure as they were eluted below the lower limit of column. Apart from linear olefins, alkenes terminated monoesters [P4-P6] were also obtained which can be further polymerized to obtain functionalized macromolecules. Isomerised linoleic acid methyl esters (C$_{19}$H$_{34}$O$_2$) [P7] was formed at the expense of terminal olefins and diesters during the ethenolysis of UCO and CO esters. As evident from the Figure 2.8, high amount of diesters were formed at catalyst loading of 20 ppm. As catalyst loading decreased, decrease in intensity of diesters peak was observed. Similar trend was also observed for the monoester component (P6) with decrease in the catalyst loading. Though the conversion and yield were shown to decrease with lower catalyst loading, high turnover numbers were obtained for 7.5 ppm as shown in Table 2.7 Further decreasing the amount of catalyst loading resulted in decrease in TONs as observed at 5 ppm of catalyst load. Thus, the optimum value of catalyst loading was determined to be 7.5 ppm for ethenolysis of UCO esters.

Table 2.7. Ethenolysis results for used-cooking-oil derived methyl esters with G2 catalyst

Entry	Catalyst	Loading (ppm)	Temperature [°C]	Hold time [min.]	*Conv. [%]	*Yield [%]	*TONs
1	G2	50	50	30	96.0	64.4	14140
2	G2	20	50	30	68.3	61.2	37930
3	G2	10	50	30	52.7	50.6	62740
4	G2	7.5	50	30	59.4	45.7	78080
5	G2	5	50	20	35.4	31.0	76880

Four different catalysts (G1, G2, HG1 and HG2) were screened for ethenolysis reaction at 50°C with 50 ppm catalyst loading. It was observed that 50 ppm G2 catalyst performed most effectively (evaluated in terms of TONs) than G1, HG1 and HG2 catalysts. Furthermore, G2 catalyst was incorporated at different loading to evaluate conversion, yield and TONs for ethenolysis of UCO esters as shown in Table 2.7. In this study, catalyst at 50 ppm loading exhibited the highest conversion and yield (96% and 64.4% respectively) which significantly reduced to 35.4% and 31% respectively when catalyst loading was lowered to 5 ppm. Highest TONs were obtained with 7.5 ppm catalyst loading which manifested 59.36% conversion and 45.75% yield. Additionally, the conversion and yield obtained at catalyst loading of 20 ppm was found to be 68.3% and 61.18% respectively with TONs enumerated as 37930. At 10 ppm, conversion was further reduced to 52.7% while the percent yield was measured as 50.6%, thereby revealing moderate TONs of 62740. The increase in conversion at 7.5 ppm in comparison to catalyst loading of 10 ppm was observed due to formation of isomerised products in substantial amount. Nevertheless, yield followed the decreasing trend with lower amount of catalyst loading.

2.3.9 Lipid composition in CF, UCO and CO esters

Table 2.8: Composition (mol %) of saturated and unsaturated lipidic components present in CF, UCO and CO esters

Lipidic Sources	Saturated Lipids		Unsaturated Lipids				
	C16:0	C18:0	C16:1	C18:1	C18:2	C18:3	Others
Chicken Fat (CF)	23%	5%	8%	40%	21%	1%	2%
Used Cooking Oil (UCO)	10.5%	2.7%	<1%	48%	33%	1.6%	3.2%
Canola Oil (CO)	3.5%	1.5%	<1%	64%	20%	10%	<1%

The GC-FID analytical method was successfully employed for simultaneous determination of numerous fatty ester components in lipidic samples of different origins (CF, UCO, CO). The contents of saturated and unsaturated lipidic components were quantified using methyl heptadecanoate (C17:0) as an internal standard. The data summarized in Table 2.8 indicates that CF contains the least proportion of unsaturated lipids (70 mole%), followed by UCO (83 mole%) and CO (94 mole%). These values are in accordance to the highest TONs achieved for various substrates(CF: 21820; UCO: 78080; CO: 92000) thereby supporting the proposed hypothesis that reactivity of Grubbs and Hoveyda-Grubbs catalyst is significantly affected by the amount of various saturated and unsaturated moieties in the feedstock. It was observed that palmitic ester (C16:1) was present in trace amount in UCO and CO, while CF predominantly contained 8 mole% of palmitic ester component. Although CF contained high proportion of saturated components, nevertheless, both CF and CO esters depicted greater activity towards HG2 catalyst. However, UCO showed higher activity towards G2 catalyst. These studies suggest that activity of catalyst is not only affected by saturated components but also dependent on the presence of other non-triglyceride components like cholesterol or tocopherol that may decompose the catalysts.

2.3.9 Visualization of ethenolyzed components on TLC plate
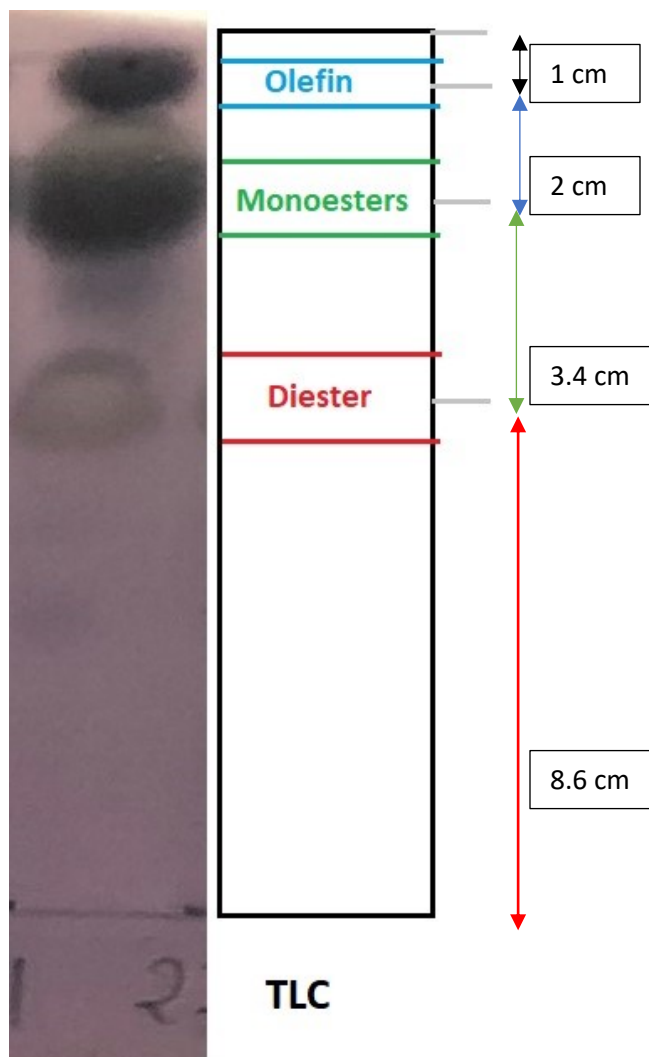
Figure 2.10: TLC for olefin, monoesters and diesters obtained after ethenolysis of fatty acid methyl esters

R_f (diester) = 8.6/15 = 0.57

R_f (monoesters) = 12/15 = 0.80

R_f (olefin) = 14/15 = 0.93

The retention factors for olefins, esters and diester were calculated as 0.93, 0.80 and 0.57 respectively.

The separation of ethenolyzed components/fractions was carried out using column chromatographic system, where silica gel was taken as a stationary phase and hexane/ethyl acetate (95/5) as a mobile phase. The column was packed using wet method where a slurry of silica and solvent(hexane) was prepared and then poured into the column using a funnel. Ethenolyzed products mixed with silica were added from the top of the column in such a way that the top level of it is not disturbed. The polar components were adsorbed on the surface of silica and the non-polar components(olefins) were eluted out in the initial stage. Separated fractions were further confirmed by FTIR to validate the successful separation.

2.3.10 ATR-FTIR spectra for separated ethenolyzed components
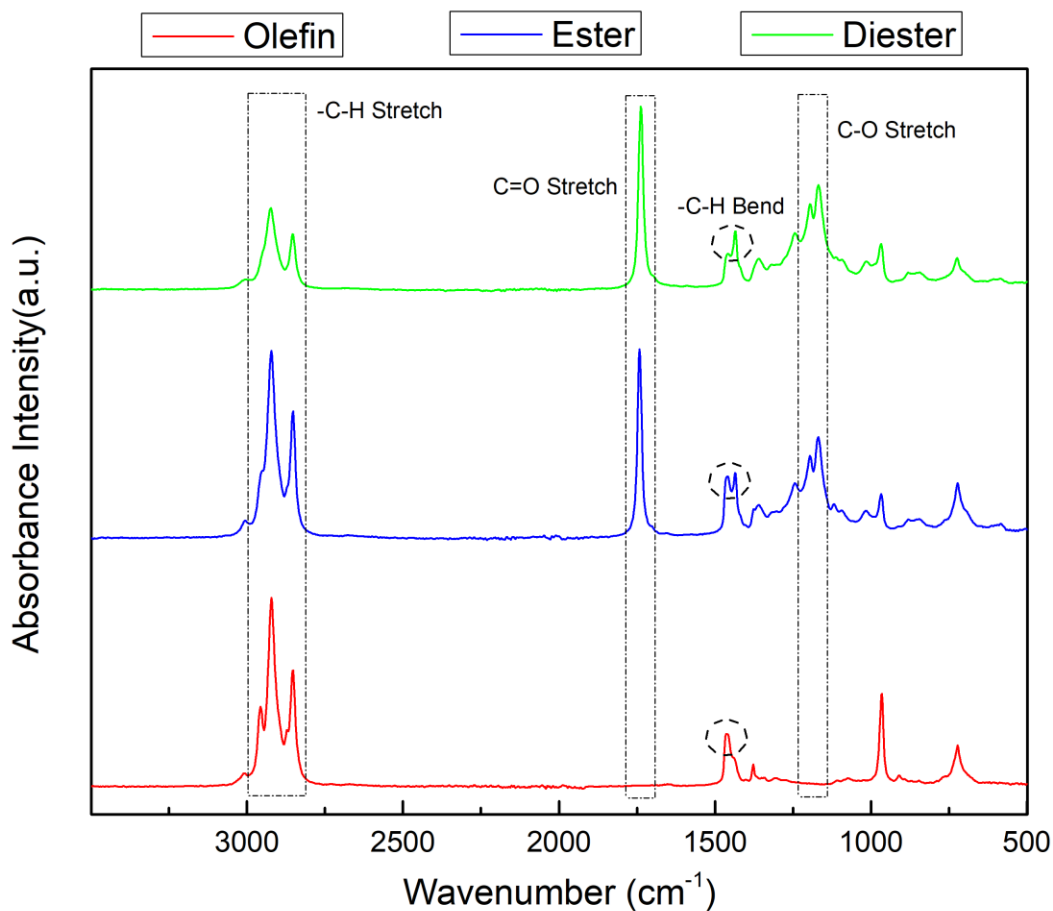
Figure 2.11: ATR-FTIR spectra for ethenolyzed components

As shown in FTIR spectra (Figure 2.11), absorbance between 1150-1220 cm^{-1} was attributed to C-O stretch and peak at 1747 cm^{-1} corresponded to carbonyl entity (C=O stretch). As expected, these peaks were observed in the case of monoesters [P4-P7 as shown in GC-MS] and diesters [P8 as shown in GC-MS], while these peaks are absent in olefinic mixture [P1-P3 as shown in GC-MS]. The distinction between esters and diesters was marked by the intensity ratio of C=O stretch to CH stretch. The absorbance intensity of C=O stretch for diesters was found to be substantially higher as compared to monoester components due to the presence of dual carbonyl peaks in diesters. In addition, the absorbance for CH bending was observed at 1409 cm^{-1} and there was noticeable change in the peak shape for three different components of olefin, monoesters and diesters respectively.

References

1. Merli, R., M. Preziosi, and A. Acampora, *How do scholars approach the circular economy? A systematic literature review.* Journal of Cleaner Production, 2018. **178**: p. 703-722.

2. Maddikeri, G.L., A.B. Pandit, and P.R. Gogate, *Intensification approaches for biodiesel synthesis from waste cooking oil: a review.* Industrial & Engineering Chemistry Research, 2012. **51**(45): p. 14610-14628.

3. Math, M., S.P. Kumar, and S.V. Chetty, *Technologies for biodiesel production from used cooking oil—A review.* Energy for sustainable Development, 2010. **14**(4): p. 339-345.

4. *Environmental Audit Committee - Green Economy: Written evidence submitted by the UK Sustainable Biodiesel Alliance*2012; Available

from:https://publications.parliament.uk/pa/cm201012/cmselect/cmenvaud/1025/1025vw0 8.htm.

5. Safder, M., F. Temelli, and A. Ullah, *Extraction, optimization, and characterization of lipids from spent hens: An unexploited sustainable bioresource.* Journal of Cleaner Production, 2019. **206**: p. 622-630.

6. Jessop, P., et al., *Opportunities for greener alternatives in chemical formulations.* Green Chemistry, 2015. **17**(5): p. 2664-2678.

7. Ullah, A. and M. Arshad, *Remarkably Efficient Microwave-Assisted Cross-Metathesis of Lipids under Solvent-Free Conditions.* ChemSusChem, 2017. **10**(10): p. 2167-2174.

8. Mol, J., *Metathesis of unsaturated fatty acid esters and fatty oils.* Journal of molecular catalysis, 1994. **90**(1-2): p. 185-199.

9. Chatterjee, A. and V.R. Jensen, *A heterogeneous catalyst for the transformation of fatty acids to α-olefins.* ACS Catalysis, 2017. **7**(4): p. 2543-2547.

10. Nieres, P., et al., *Heterogeneous catalysis for valorisation of vegetable oils via metathesis reactions: ethenolysis of methyl oleate.* Catalysis Science & Technology, 2016. **6**(17): p. 6561-6568.

11. Spekreijse, J., et al., *Simultaneous production of biobased styrene and acrylates using ethenolysis.* Green Chemistry, 2012. **14**(10): p. 2747-2751.

12. Park, C.P., et al., *Low pressure ethenolysis of renewable methyl oleate in a microchemical system.* Organic letters, 2011. **13**(9): p. 2398-2401.

13. Song, J., et al., *Effect of phase behavior on the ethenolysis of ethyl oleate in compressed CO2.* The Journal of Physical Chemistry B, 2009. **113**(9): p. 2810-2814.

14.   Ashworth, I.W., et al., *Olefin metathesis by grubbs–hoveyda complexes: computational and experimental studies of the mechanism and substrate-dependent kinetics.* Acs Catalysis, 2013. **3**(9): p. 1929-1939.

15.   Burdett, K.A., et al., *Renewable monomer feedstocks via olefin metathesis: Fundamental mechanistic studies of methyl oleate ethenolysis with the first-generation Grubbs catalyst.* Organometallics, 2004. **23**(9): p. 2027-2047.

16.   Arshad, M., S. Saied, and A. Ullah, *PEG–lipid telechelics incorporating fatty acids from canola oil: synthesis, characterization and solution self-assembly.* RSC Advances, 2014. **4**(50): p. 26439-26446.

Chapter 3: Biobased Polyester from waste and renewable lipids

3.1 Background

There is a dearth of development in bio-based polymeric materials for everyday-life objects such as packaging materials, especially bottles, textiles, coating, and toners, among many other uses. Several strategies have been adopted commercially to produce partially or fully bio-based plastic products(Caillol et al., 2012; Dai et al., 2015; Haq et al., 2009; Haq et al., 2008; Liu et al., 2014). For instance, Coca-Cola Company manufactures plastic bottles consisting of 30% renewable material, where ethylene glycol is substituted with bio-based ethylene glycol(Sousa et al., 2015). The strength in commercially available polyester bottles is achieved through the incorporation of rigid aromatic rings in the backbone of long polymer chain. Furan derived diols/diacids/diesters exhibit a close resemblance to commercially used aromatic diols/diacids/diesters (such as terephthalic acid used in making PET bottles). Therefore, the exploration of furan derived monomers was performed to obtain a renewable alternative to fossil-based aromatic homologs. It is expected that the mechanical strength and thermal characteristics of synthesised polymers can be enhanced by the structural feature of furan derived compounds. Gomes at al. synthesised Poly(2,5-furan dicarboxylate) based on a variety of Diols such as Ethylene glycol (99%), propane-1,3-diol (99%), 1,4-di-(hydroxymethyl)-benzene (99%) and hydroquinone (99.5%)(Gomes et al., 2011). Though several bio-based molecules demonstrated great potential at an academic stage, only few are explored at a pilot scale. Bio-based Poly (ethylene 2,5-furandicarboxylate) (PEF) is being produced at pilot scale for the development of packaging applications for soft drinks, water and alcoholic beverages, among other applications, for example as films and fibres. In the Avantium process, 5-(methoxymethyl)-2-furfural is converted into FDCA in a single step. This bio-derived 2,5-furandicarboxylic acid (FDCA) resembles very closely the petrochemical

counterpart terephthalic acid (TPA), notably the aromatic ring with two carboxylic groups in opposite positions. PEF is now industrially produced in Geleen, The Netherlands based on Avantium YXY technology(Sousa et al., 2015). At this point, it is important to understand the underlying chemistry of these resembling molecules. Terephthalic acid contains 6-membered aromatic ring (phenylene ring) whereas FDCA consist of 5-membered aromatic ring (furan ring). The aromaticity is substantially higher for phenylene ring as compared to furan ring. This aromaticity leads to greater covalent strength along the chain axis. Another important parameter that contributes toward covalent strength is lone electron pairs of oxygen atoms. Thus, the reduction in covalent strength for furan is counterbalanced by the presence of lone pair of electrons, thereby maintaining the strength and overall interactions among polymeric chains.

Furthermore, the effect of ring motions was compared in earlier studies between furan rings and phenyl rings as illustrated in Figure 3.1. The restrictive ring-flipping motion in 5-membered furan ring is believed to positively contribute towards reduction in oxygen diffusion coefficient (0.0107 for PEF vs. 0.114 for PET) and oxygen permeability (1.04 cm^2 s^{-1} for PEF vs. 11.60 cm^2 s^{-1} for PET). The chain relaxation was quantified with the help of glass transition temperature where higher T_g was observed for PEF (86°C) as compared to PET(76°C)(Burgess et al., 2014). Thus, the superior barrier properties of PEF as compared to PET make it a preferential choice for food and beverage packaging applications such as bottles.
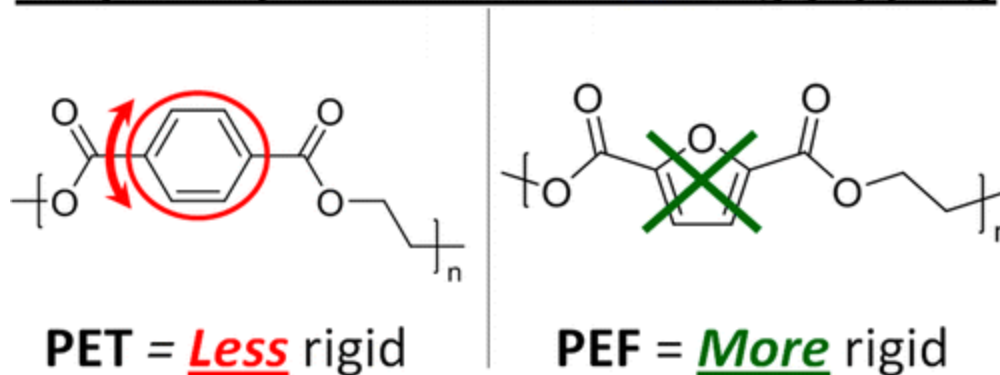
Figure 3.1: Dependence of polyester rigidity on ring-flipping motion {Adapted with permission from Chain Mobility, Thermal, and Mechanical Properties of Poly(ethylene furanoate) compared to Poly(ethylene terephthalate). Copyright © 2014, American Chemical Society.

Another important parameter that is intensively analysed is the extent of hydrophobicity of the sample. The contact angle with water (θ_w) on the PEF flat specimen was determined by Burgess et al. to be equal to 67° suggesting a somewhat polar character(Burgess et al., 2014; Sousa et al., 2015).

Apart from chemo-catalytic routes to synthesize polyesters(Elliot et al., 2017; Le Roux, 2016; Li et al., 2019), enzymatic routes have also been incorporated in previous studies(Fodor et al., 2017; Pellis et al., 2016). Loos et al. in 2015 reported the use of Candida Antarctica lipase B and mild reaction temperatures (80 or 40 °C respectively) that complements principles of green chemistry to certain extent. However, high amount of energy was consumed in this enzymatic approach due to longer reaction time involved (24–72 h). Moreover, the molecular weight for the final product obtained using enzymatic route was very low (around 2000 g mol^{-1} or less)(Jiang et al., 2014).

The furan counterpart of PET is reported in earlier studies where, 2,5 furan dicarboxylic acid dichloride and ethylene glycol were employed to obtain polyester with glass transition temperature

(T_g) between 75-80 °C, crystallization temperature (T_c=165 °C) and melting point (T_m) between 210-215 °C. Small amount of aqueous HCl was added during the bulk polymerization and antimony oxide was used as a catalyst for step-polymerization at 70-220°C(Gandini et al., 2009). FDCA polyesters with longer aliphatic chains can present alternative properties such as fast crystallization or toughness(Guigo et al., 2019).

In our present study, fully biobased polyester was synthesized using antimony oxide as the catalyst. Moreover, 10% 3,4-Bis(hydroxymethyl)furan was used to incorporate rigid aromatic moieties in the main chain of polyester.

3.2 Experimental Section

3.2.1 Materials

Used cooking oil (96.8%). Grubbs catalyst 2nd generation (G2, 97%), Antimony(III) oxide (≥99%), 3,4-Bis(hydroxymethyl)furan(98%), Lithium aluminium hydride (powder), potassium hydroxide (≥ 85 %), sodium chloride (≥99.5 %), anhydrous sodium sulfate (≥99%), methanol (≥99.8 %) were obtained from Sigma–Aldrich. Ethylene gas (Praxair Inc., 99.9 %), silica gel used for column chromatography (70–230 mesh, 60 Å pore size), flash silica (Silicycle, 40–63 mm, 230–400 mesh), thin layer aluminium chromatographic plates (Sigma-Aldrich, 0.20 mm thick, 20×20 cm size, binder polymeric, fluorescent indicator), ethyl acetate (Fisher, 99.9 %), and n-hexane (Caledon) were purchased and used as received.

3.2.2 Methods

3.2.2.1 Diester and diol synthesis: All the metathesis reactions were performed on a customized microwave (Matthews, USA), in a 500 mL batch scale-up pressure reactor. The cylindrical vessel (15 cm outer diameter, 17 cm maximum height and 2 cm wall thickness) was made from PEEK

material with the operating limits of 250°C and 100 psi. The reactors were purged with N_2 prior to transfer of methyl esters. The quantity of methyl esters varied between 100-150 g and corresponding amount was catalyst was calculated to maintain its' concentration at 50 ppm. Catalyst was transferred to the reaction vessel inside the glove box (with flow of nitrogen) to eliminate every trace of oxygen. The vessel was sealed and then placed inside the microwave system. The pressure of ethylene (60 psi) was applied and the reactions were heated (50°C) and stirred during the reaction time (30 minutes). Air stirrer ensured homogenous mixing of catalyst and feedstock, while temperature probe was used to monitor temperature changes during the reaction. Outer channels of gas pipes and temperature probe was sealed with Teflon tape to avoid any leakage of components during the ethenolysis process. After the reaction, the reactors were opened, and an aliquot was filtered over a plug of silica prior to their injection into the GC-MS. 9-octadecene-1,18-diol (diol) was synthesised by following an earlier reported procedure (Quinzler & Mecking, 2010)

3.2.2.2 Polymerization step: 8.8 mmol diol and equivalent diester were added into a 25 mL round bottom flask, followed by 1.0 mol% Antimony Oxide catalyst. After initial condensation reaction at 80 °C for two hours, reaction temperature was gradually raised up to 200 °C at a rate of 30°C/60 min and the step-polymerization was carried under reduced pressure. The reaction was stopped after 4 h to obtain yellow solid. The obtained polyesters were thoroughly washed in cold methanol and dried before proceeding for various analyses.

3.2.3 Characterization

GC-MS analyses of all samples were conducted on Agilent 6890N (USA) gas chromatograph fitted with a fused silica capillary column SP2560 (100 m *0.25 mm, 0.2 μm film thickness) linked to a detector 5975B inert XL MSD. A sample volume of 2 mL was injected, the injector temperature

was set to 240 °C and a split mode with ratio of 20:1 was used. The temperature profile was held at 45 °C for 4 min; then increased to 175 °C (13 °C min^{-1}) and held for 27 min; and further ramped at 4 °C min^{-1} to 215 °C and held for 35 minutes. Helium gas was used as mobile phase with a constant flow rate of 1.3 mL min^{-1}.

The composition of ethenolyzed products was evaluated with GC-FID analysis by calculating corresponding area at retention time of each component. GC-FID analyses were conducted on PerkinElmer GC-FID Clarus 500 instrument (USA) equipped with flame ionization detector. The temperature was set at 280 °C for the detector and 240 °C for the injector. Air and hydrogen were used as carrier gases with flow rates of 450 and 45 mL min^{-1}, respectively. The column used and all other conditions were as mentioned above for GC-MS instrument Agilent 6890N.

Moreover, the components were analysed in TLC plates, then separated into olefins, esters and diesters fraction by column chromatography. The separation was performed in column chromatographic system that used silica gel as a stationary phase and hexane/ethyl acetate (95/5) as a mobile phase. The column was packed using wet method where a slurry of silica and solvent(hexane) was prepared and then poured onto the column using a funnel. Metathesized products mixed with silica were added from the top of the column in such a way that the top level of it is not disturbed. The polar components were adsorbed on the surface of silica and the non-polar components(olefins) were eluted out in the initial stage. Separated fractions were further confirmed by FTIR to foster the validity of the separation.

ATR-FTIR spectra of the ethenolyzed components were recorded using a Bruker Optics (Esslingen, Germany) unit equipped with a single bounce diamond ATR crystal. All samples were scanned in the wavelength range of 400 - 4000 cm^{-1}. Spectra were obtained using OPUS software version 6.5 from Bruker and a total of 16 scans at a resolution of 4 cm^{-1} were recorded for each

sample. Background scans (16 scans) were also performed manually before each fraction was analysed.

NMR spectra: Samples for solution NMR studies were prepared by dissolving 15 mg of polymer in 0.7 mL of chloroform-d in a standard 5 mm NMR tube. 1H NMR was carried out at room temperature by a Varian INOVA at the frequencies of 400 MHz. Chemical shift values were determined by referring to the signal of the solvent, set at 7.26 ppm in the ^{1}H spectrum.

Gel Permeation Chromatography (GPC): The average molecular weights (Mw's) of prepared polyesters were determined by gel permeation chromatography. A Phenogel™ 5 μm 10E4A, LC Column (4.6 mm × 300 mm) and 2000 ELSD detector were equipped with the GPC instrument. The samples with a concentration of 0.5 mg/mL in THF were used, where THF was used as an eluent with a flow rate of 0.350 mL/min. A series of polystyrene standards were used to calibrate the instrument.

Thermal properties: The melting temperature and glass transition temperature of polymerized samples were investigated using a calorimetric apparatus (2920 Modulated DSC, TA Instrument, USA) in a continuous flowing nitrogen atmosphere. The instrument was calibrated for heat flow and temperature using a sample of pure indium. All samples were scanned at a heating rate of 5°C per minute in a temperature range of -20°C to 150°C. The thermal stabilities of the specimen were studied using TGA Q50 (TA Instrument, USA) under a continuous nitrogen flow between 25 and 600°C at a heating rate of 10°C/min.

Film Preparation: For polyester film preparation, the polyesters (~1.5 g) were crushed in a mortar and then taken on steel plates for compression molding. A Carver press was used to press the samples, where a pressure of 1000 psi were applied for 10 min. The temperature of upper plate

was maintained at 35°C while lower plate was heated to 40°C and plates were covered with the Krapton film to ensure material sticking of the material. This approach helped to achieve uniformity in film thickness and lead to protection against film breakage during plate removals.

Film Thickness: Digital caliper (Digi-Max Caliper, Sigma-Aldrich, USA) was used to measure thickness and width of the films at three different places, and the values were averaged.

Thermal Property Measurement: The thermal stabilities of the specimen were studied using TGA Q50 (TA Instrument, USA) under a continuous nitrogen flow between 25 and 600°C at a heating rate of 10°C/min.

Injection Moulding: The polymerized samples were moulded using a lab-scale injection moulder (HAAKE MiniJet System, Thermo Electron Corporation, Karlsruhe, Germany). An injection pressure of 150 bar during 10 s was used to prepare specimen using two types of mould (557-2293 mould Disc (D: 35 mm / H:1.5 mm) and 557-2299 Tensile Bar Typ V) (ASTM D638). The temperature of the mould was set at 50°C. After cooling, flat dumbbell shaped and disk-shaped specimen with a mass of 1.5g were obtained.

Mechanical Property measurement: Tensile properties (tensile strength and elongation to break) of the films were measured in triplicate at room temperature using a universal testing machine (Autograph AGS-X Shimadzu, Canada) following ASTM standard method D822. The averaged specimen dimensions were 50 mm × 9mm × 0.3mm (length × width × thickness). A 50 N load cell with a crosshead speed of 1.0 mm/s was used. Before testing, samples were equilibrated at 25°C and 65% relative humidity (RH) for 48 h.

3.3 Results and Discussion

3.3.1 Synthesis of diesters from UCO

Diesters were obtained with G2 catalyst using the same procedure mentioned in Chapter 2. Figure 3.3 below illustrates GC-FID spectra for various components obtained after metathesis reaction while Figure 3.2 depicts GC-FID spectra for the feedstock. 20% yield of diester was obtained that was separated using column chromatography as mentioned earlier.
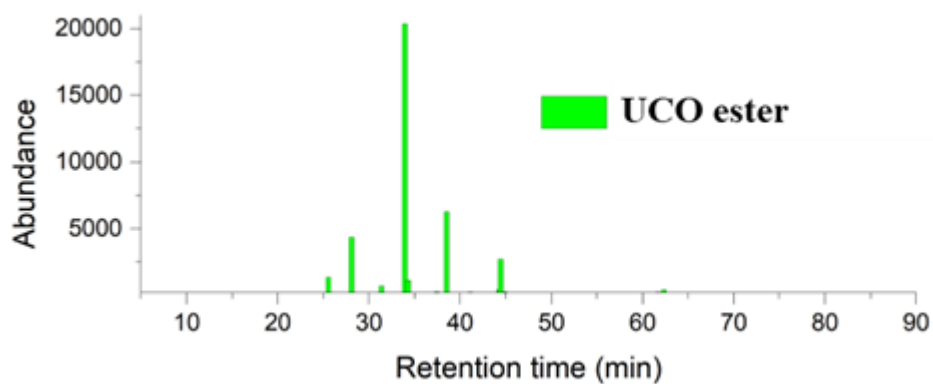

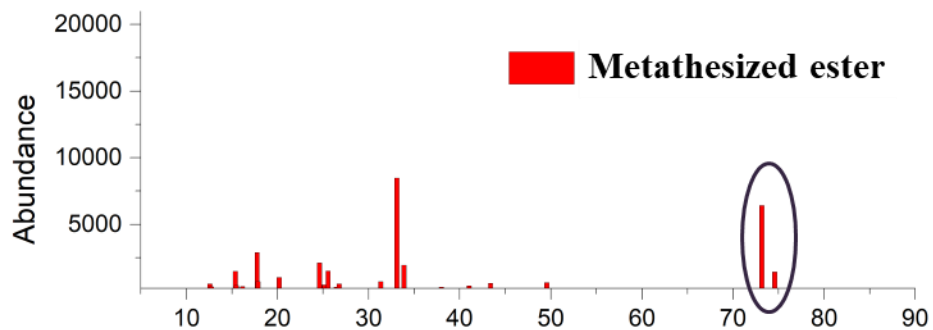*Figure 3.2: GC-FID spectra of UCO esters*

Figure 3.3: GC-FID spectra metathesized products from UCO with 50 ppm G2 catalyst

3.3.2 Synthesis of 9-octadecene-1,18-diol

9-octadecene-1,18-diol (diol) was synthesised by following an earlier reported procedure (Quinzler & Mecking, 2010). 0.0382 moles of dimethyl-9-octadecene-1,18-dioate (13 g) was dissolved in 70 mL THF. 3.04 g LiAlH$_4$ was suspended in 40 mL dry THF and added slowly (dropwise) to the cooled flask containing diester. After further addition of 10 mL THF, the slurry was stirred at 700 rpm. The reaction mixture was refluxed for 1 hour and then stirred overnight at room temperature. Sequentially, 0.5 mL water, 0.5 mL 15% aqueous NaOH solution and 0.5 mL water were slowly added to quench the reaction. The white precipitate was filtered out at 40 °C and the solvent was removed from the filtrate under reduced pressure. The resulting solidified product (9-octadecene-1,18-diol) was obtained with 85% yield and characterization was performed using FTIR and NMR technique. The scheme 3.1 for the synthesis is illustrated below.
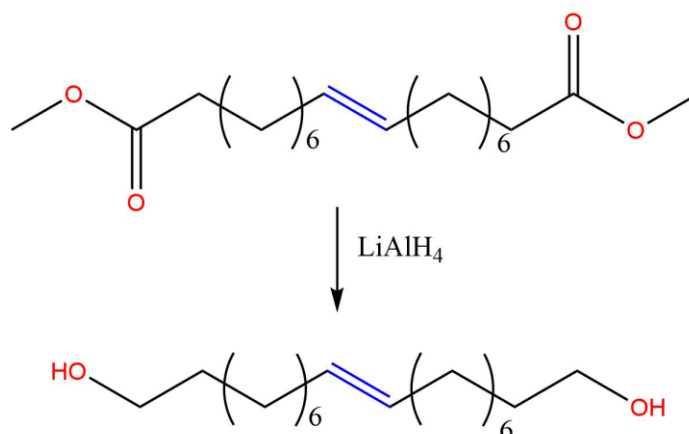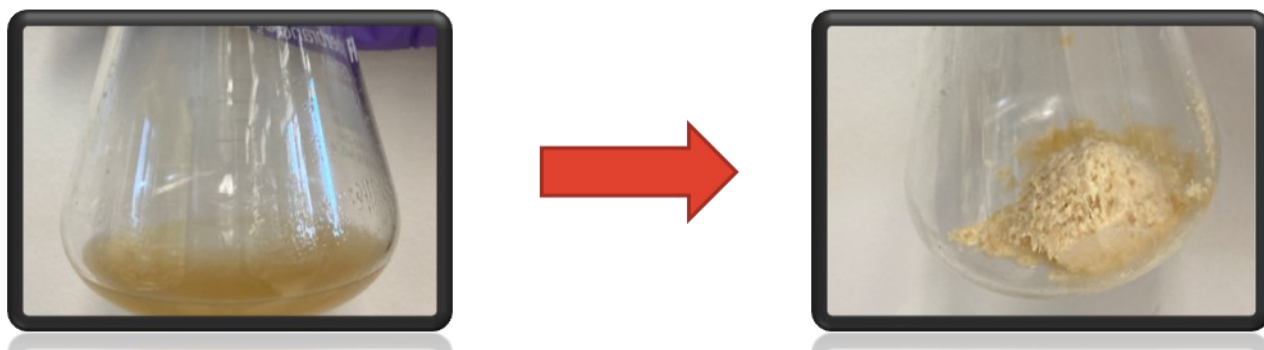

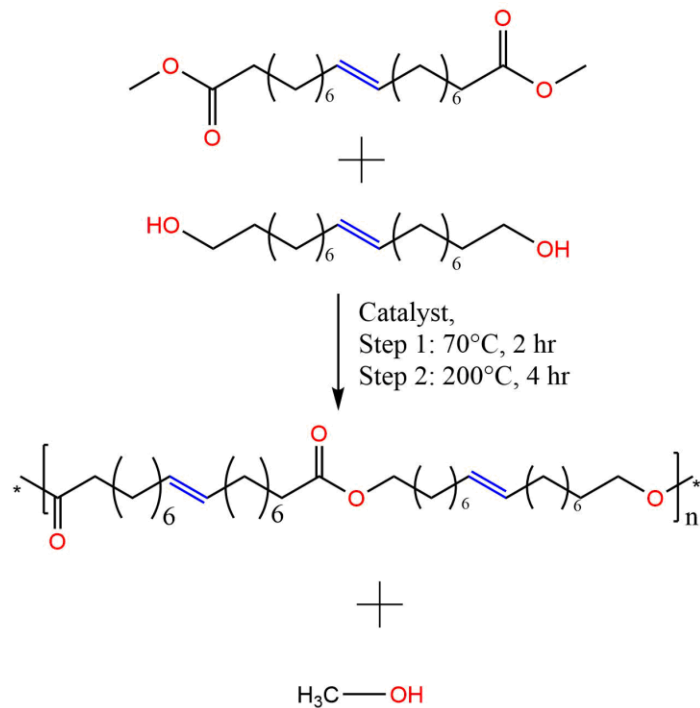*Scheme 3.1: Synthesis of 9-octadecene-1,18-diol*

3.3.3 Polycondensation reaction of diester and diol

Polyester was synthesized using condensation polymerization technique by incorporating antimony oxide as a catalyst. Diester monomer (2.5 g, 73.4 mmol), diol monomer (2.2 g ,73.4 mmol), and catalyst (40 mg, 0.13 mmol) were taken ina 25 mL dry round bottom flask and condensation

reaction was performed for 2 hours prior to polymerization reaction, after purging the reaction mixture with nitrogen for 15 min. The reaction vial was finally heated to 210 °C under vacuum. The reaction was performed for the duration of 4 hours. The viscous nature of the synthesised polymer was marked by observing change in the rate of stirring. The reaction flask was exposed to air followed by precipitation in cold methanol at least three times (from THF solution) to remove remaining monomer and all other contents as shown in Figure 3.4. The collected polymer was dried in a vacuum oven (25 mm Hg) at room temperature to obtain yellowish sticky polymer with ~75% yield. The scheme 3.2 for polyester synthesis is highlighted below.

Figure 3.4: Precipitation of synthesized polyester in cold methanol to obtain polymer flakes

Scheme 3.2: Polyester synthesis from 9-octadecene-1,18-diester and 9-octadecene-1,18-diol

3.3.4 Detailed analysis of synthesized compounds

Polyesters displayed very high molecular weights (Mw's) as shown in Figure 3.7 and Figure 3.8 below as analysed with the help of gel permeation chromatography (GPC) . The molecular weight obtained using GPC was calculated as 506.07 g/mol for 9-octadecene-1,18-diester (Figure 3.5), 446.62 g/mol for 9-octadecene-1,18-diol (Figure 3.6). Bimodal molar mass distribution was observed for the synthesized polyesters with both the catalyst system antimony oxide as well as tin chloride. Synthesis route with tin chloride possessed higher molecular weight (66209 g/mol versus 48408 g/mol with antimony oxide). However, by comparing the peak intensity ratio of the two peaks within the same system, the higher ratio (Peak 1/ Peak 2) was observed for the system using antimony oxide. This indicates high proportion of polyester segments for Mw= 48408 with respect to Mw = 18804 for antimony oxide system. On the other hand, the use of tin chloride lead

to the formation of polyester with molecular weights 66209 and 15038 respectively with predominantly greater proportion of later molecular weight. Moreover, discoloration (black color) was observed while using tin chloride possibly because of side reactions during polyester synthesis. Therefore, antimony oxide was selected to perform condensation polymerization reaction between 9-octadecene-1,18-diester and 9-octadecene-1,18-diol.
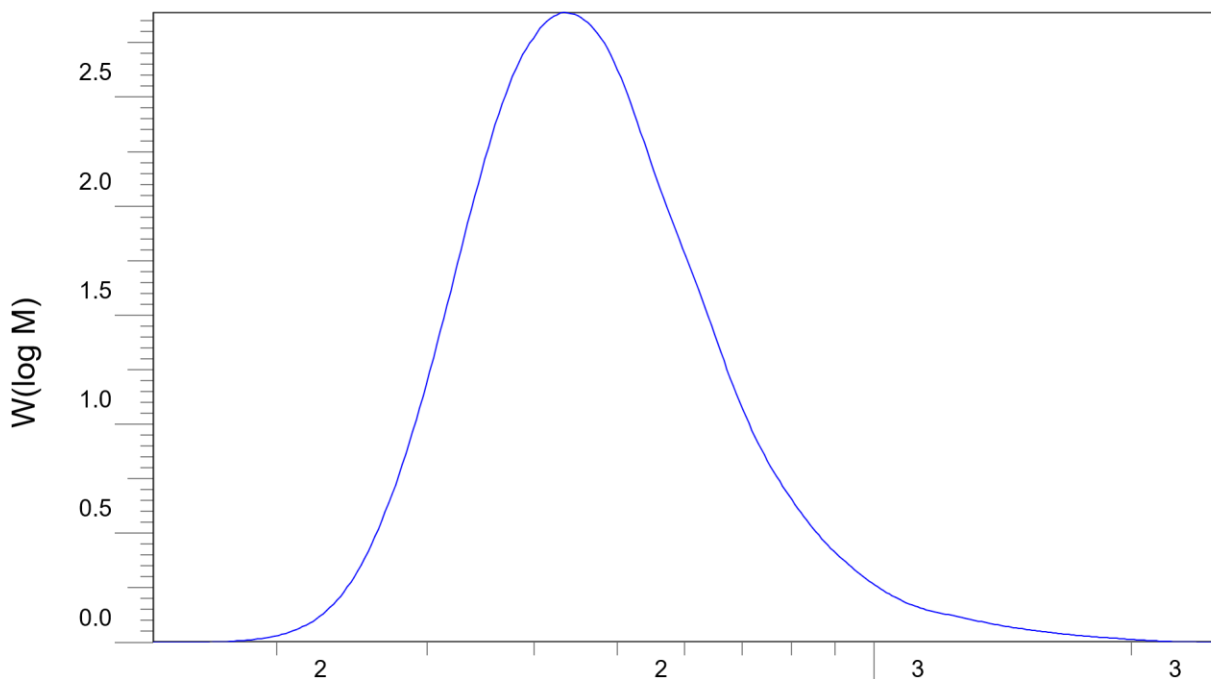
Figure 3.5: Chromatogram obtained for 9-octadecene-1,18-diester in GPC with Mw = 506.07 g/mol
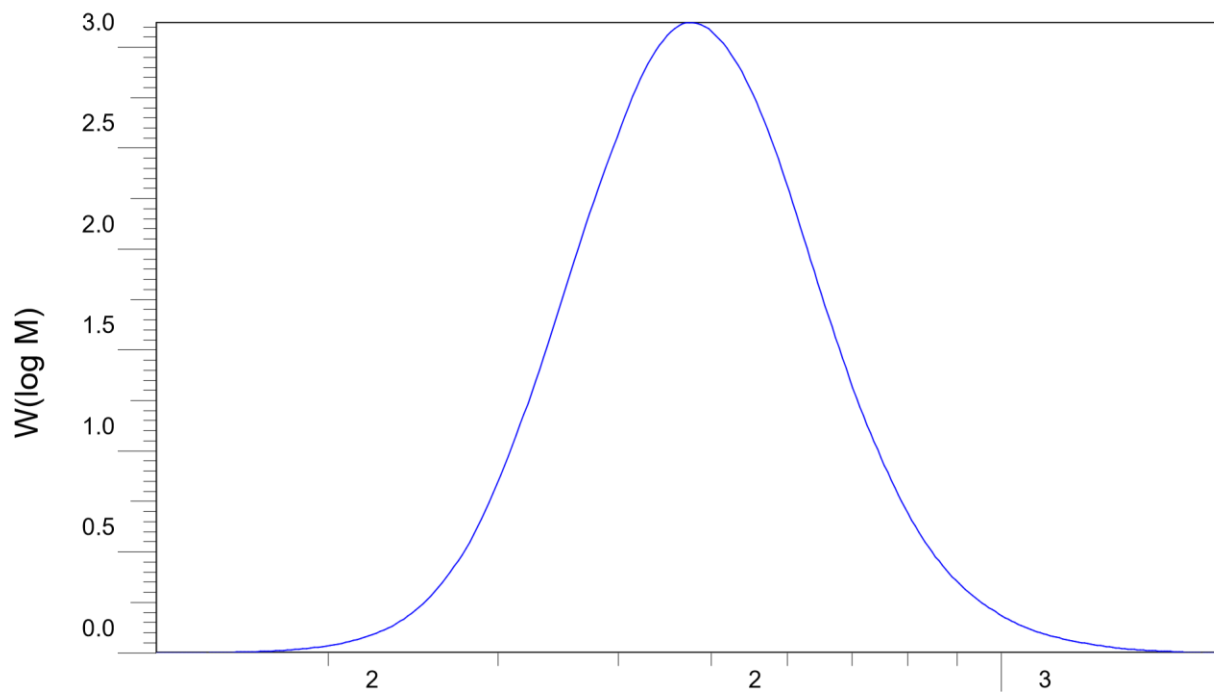
Figure 3.6: Chromatogram obtained for 9-octadecene-1,18-diol in GPC with Mw = 446.62 g/mol
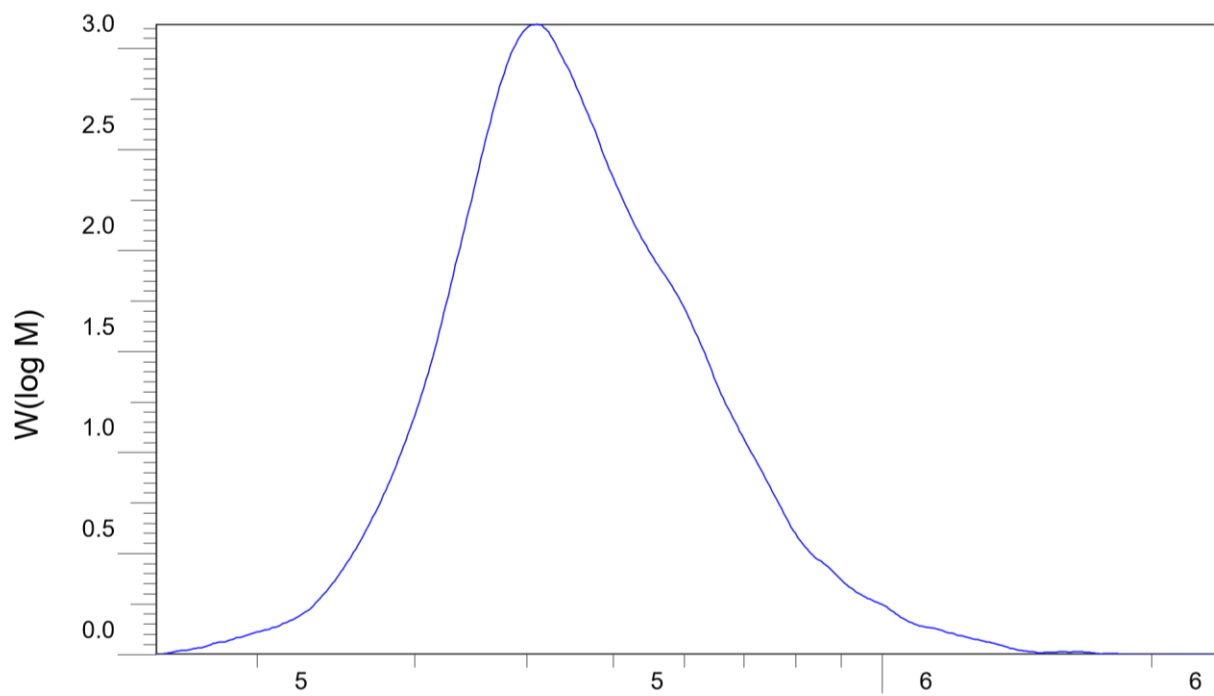
Figure 3.7: GPC chromatogram obtained for polyester obtained using Antimony oxide as catalyst with Mw = 48408 g/mol
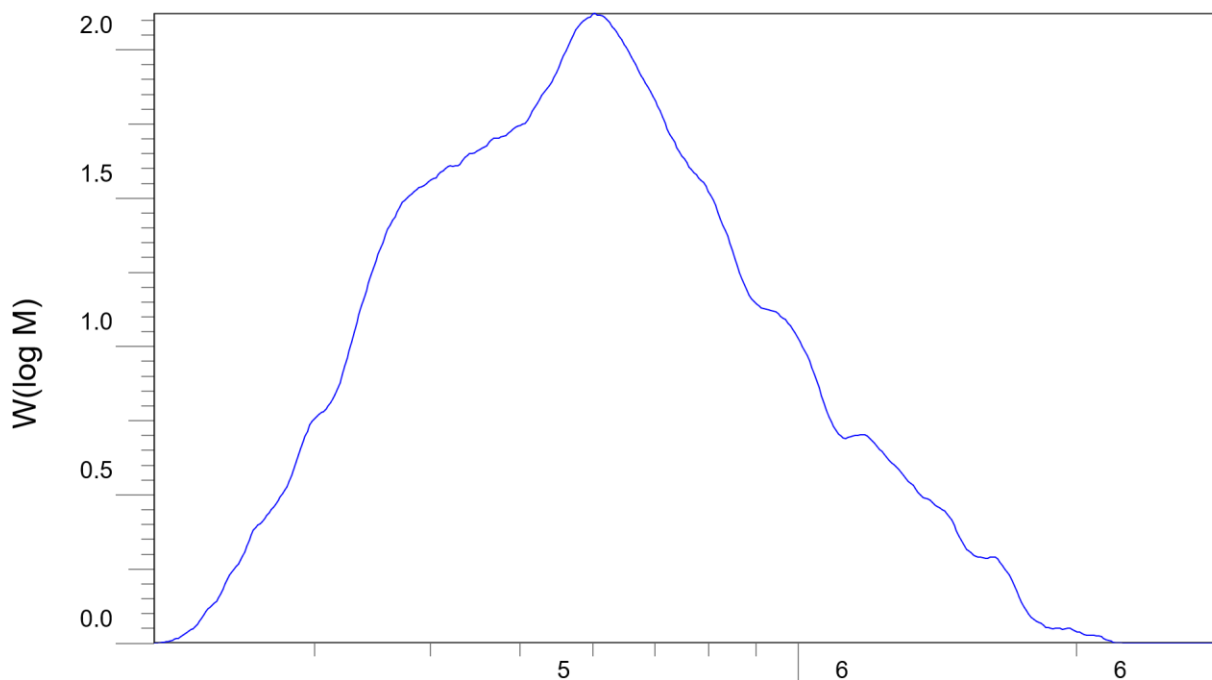
Figure 3.8: GPC Chromatogram obtained for polyester obtained using Tin chloride as catalyst with Mw = 66209 g/mol

The chemical moieties in the samples were confirmed using ^{1}H NMR.

Diol: ^{1}H NMR (400 MHz, *solvent CDCl₃*) d ppm 7.28 (s, 1H), 5.49-5.31 (m, 1H), 3.66 (dd, *J* = 9.75, 6.24 Hz, 1H), 2.74 (s, 1H) , 2.14-1.92 (m, 1H), 1.59 (p, *J* = 6.71, 6.71, 6.69, 6.69 Hz, 1H), 1.37 (t, *J* = 27.57, 27.57 Hz, 1H)

^{1}H NMR spectra clearly indicate the complete conversion from diester (Figure 3.10) to diol (Figure 3.9). The methyl peak for diester at 2.32 ppm fully disappeared and the singlet peak for methyl

protons attached adjacent to oxy group at 3.65 ppm transformed into a triplet that confirmed the formation of 9-octadecene-1,18-diol.
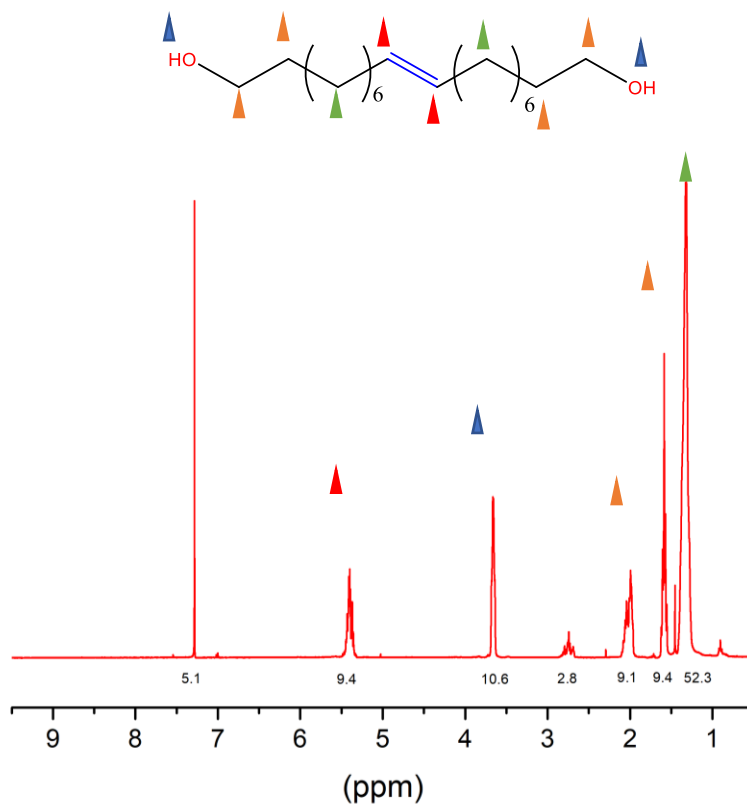
Figure 3.9: 1H NMR spectra for 9-octadecene-1,18-diol

Diester: ^{1}H NMR (400 MHz, *solvent CDCl$_3$*) d ppm 7.28 (s, 1H), 5.47-5.30 (m, 1H), 3.69 (s, 1H), 2.32 (t, J = 7.55, 7.55 Hz, 1H), 2.16-1.91 (m, 1H), 1.73-1.53 (m, 1H), 1.31 (d, J = 2.48 Hz, 1H)

Two signals at 3.66 ppm and 2.32 ppm were detected which correspond to the two methyl and methylene protons attached directly to the ester moiety of a diester (Figure 3.10). Signals between 1.31 – 2.32 ppm was attributed to the group of methylene protons far away from carbonyl moiety.
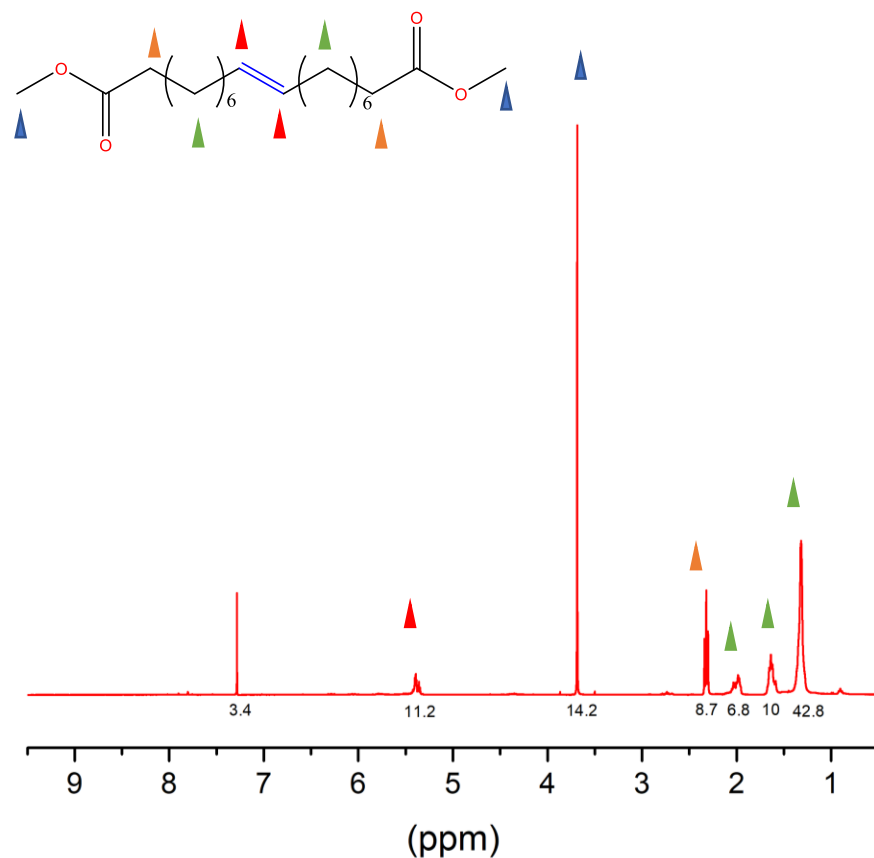
Figure 3.10: 1H NMR spectra for 9-octadecene-1,18-diester

Aliphatic polyester: ^{1}H NMR (400 MHz, *solvent CDCl₃*) d ppm 7.28 (s, 1H), 5.40 (s, 1H), 4.07 (t, *J* = 6.75, 6.75 Hz, 1H), 3.69 (s, 1H), 2.31 (t, *J* = 7.50, 7.50 Hz, 1H), 1.99 (s, 1H), 1.71-1.50 (m, 1H), 1.32 (d, *J* = 2.30 Hz, 1H)

By comparison to ^{1}H NMR spectra of diol and diester, the peak at 3.69 was attributed to the residuals of ester and hydroxyl terminal groups (as -OCH₃ and -OH). The new peak at 4.07 ppm in (Figure 3.11) correspond to the methylene protons attached directly to the alkoxy group at one end and long hydrophobic methylene moiety (from diol) at its other end.
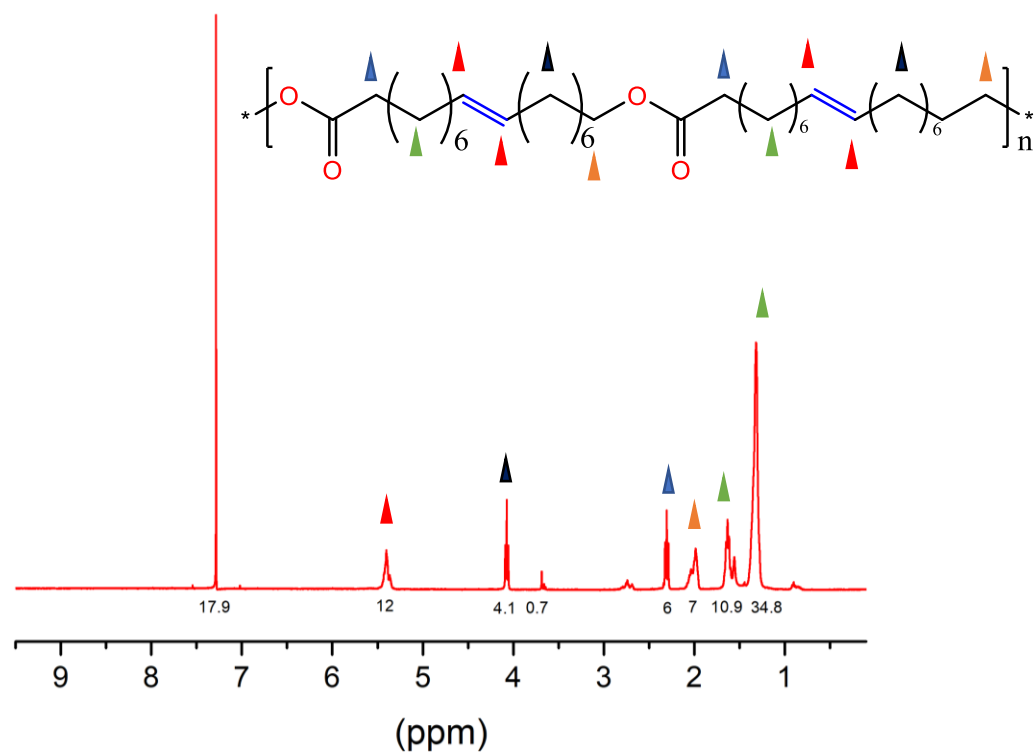
Figure 3.11: 1H NMR spectra for polyester obtained from 9-octadecene-1,18-diester and 9-octadecene-1,18-diol
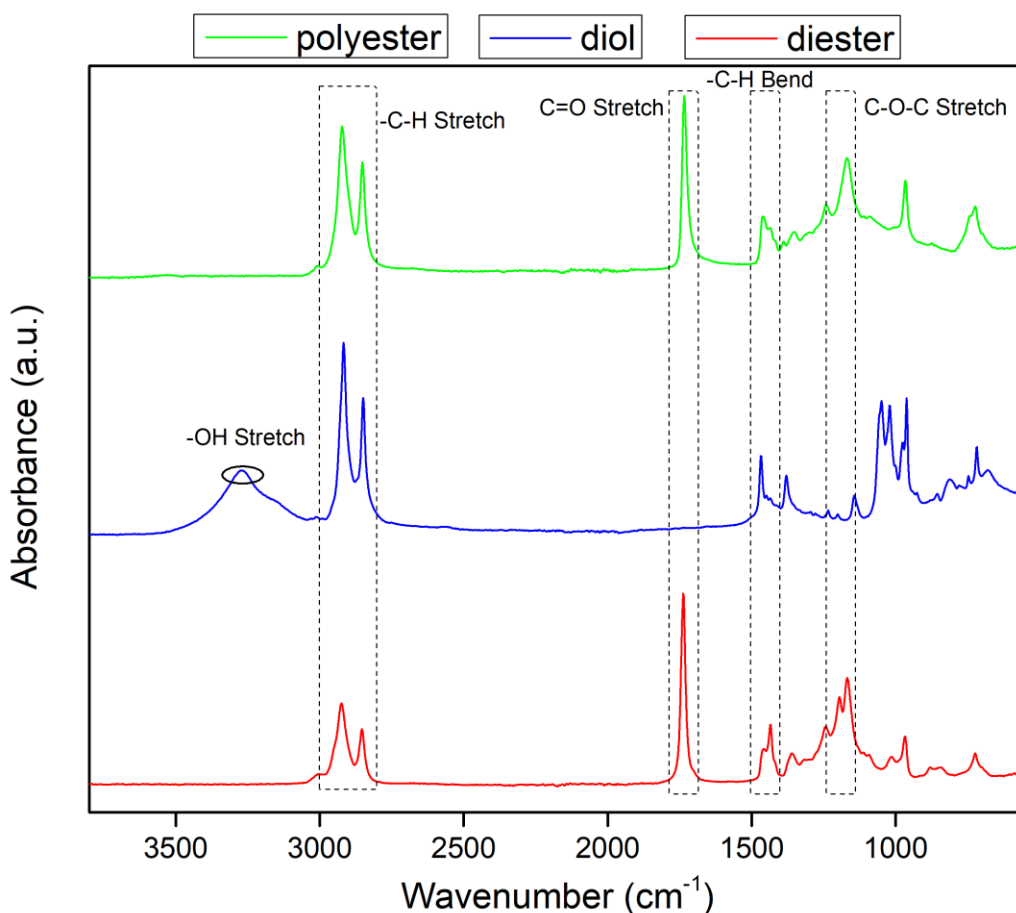
Figure 3.12: ATR-FTIR spectra for 9-octadecene-1,18-diester, 9-octadecene-1,18-diol and polyester

The formation of diester, diol and polyester were confirmed by using ATR-FTIR analysis. As shown in Figure 3.12, absorption band in the diester spectrum between 1150-1220 cm^{-1} was attributed to C-O-C stretching of diester compound and this absorption band is also evident in polyester main chain as well. However, this stretching band has been disappeared in the case of diol due to the conversion of ester group to hydroxyl group. Alternatively, broad -OH stretch at 3310 cm^{-1} was observed in the spectrum of diol. The peak at 3310 cm^{-1} was not observed in polyester spectra that signifies consumption of most diol moieties and it also manifest effectiveness of the washing step. Moreover, stretching band due to carbonyl entity (C=O stretch) was observed

at 1728 cm^{-1} for diester and polyester spectra. The aliphatic C-H stretches aliphatic main chains were observed at 2922 and 2855 cm^{-1}. In addition, the absorbance for C-H bending was observed at 1409 cm^{-1} for all the three moieties. Furthermore, the extent of polymerization was estimated from the ratio of the intensity of C=O stretching band (I_{1728}) and the C-H stretching band (I_{2922}) for diesters and polyester chains. For diester, the ratio of I_{1728}/I_{1030} was calculated as 2.5 whereas polyester chain exhibited intensity ratio of 1.2. The decrease in intensity values suggested successful incorporation of long olefin chains (from diols) that contributed towards intensified absorbance peak for C-H stretch at 2922 cm^{-1}.

After the confirmation of chemical functionality in the samples, the next step was to evaluate thermal properties using TGA and DSC.
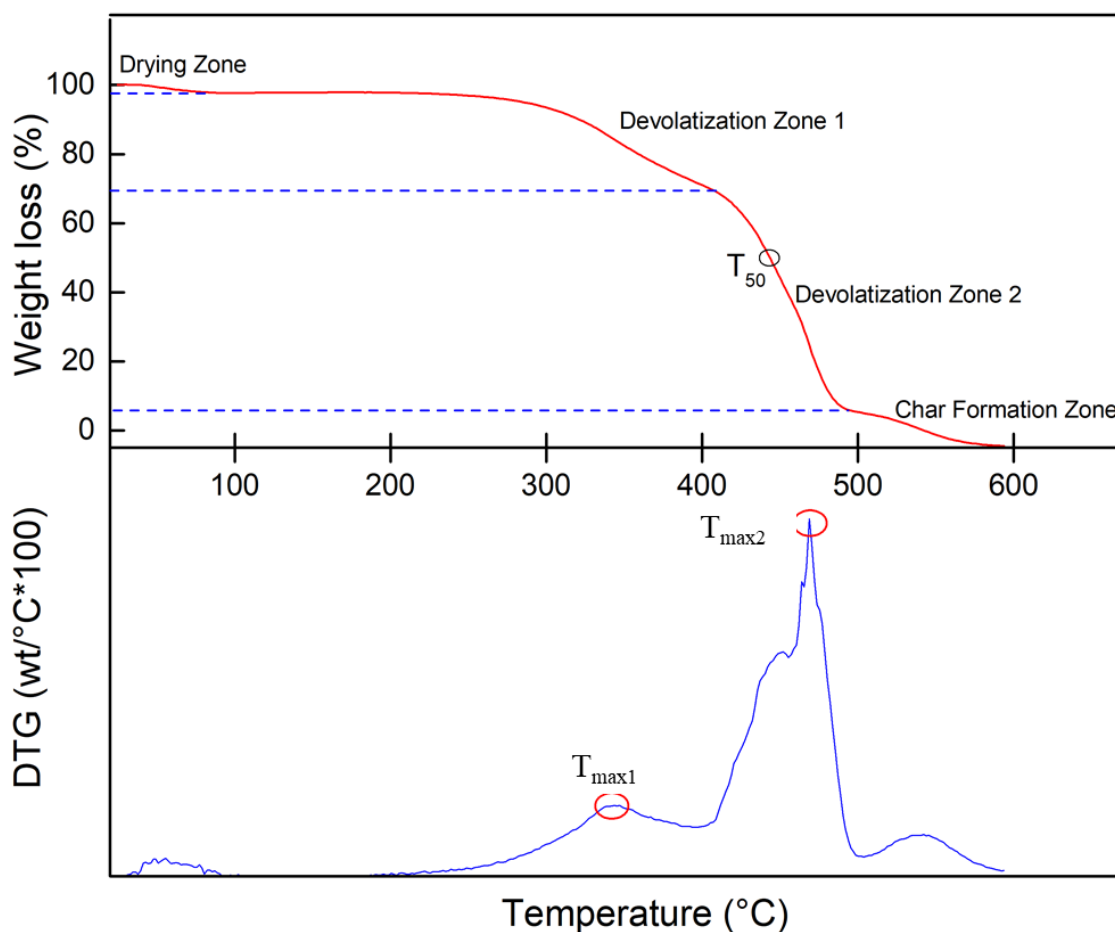
Figure 3.13: TGA analysis for polyester obtained from 9-octadecene-1,18-diester and 9-octadecene-1,18-diol

The polyester obtained after condensation of diol and diester using antimony oxide as a catalyst demonstrated initial weight loss maxima at T_{max1}=340°C, where it is speculated that short oligomers are degraded in the devolatization zone 1. At T_{50} =443°C, 50% of the sample was subjected to thermal decomposition and maximum weight loss was observed at T_{max2} = 467°C as shown in Figure 3.13. The polyester remained under continuous degradation up to 490°C with a final weight loss of 100%. The higher thermal stability of polyester and its degradation at a higher

temperature corresponds to a high molecular weight and strength of polyester. The differential form (DTG curve) is the derivative of the TG curve with respect to time that is plotted against temperature(Vyazovkin, 2002). The three DTG (derivative) peaks indicate that the process includes three mass loss steps. Multistage decomposition was observed; however, no intermediates was noted. The char formation zone occurs above 500°C indicating rupture of carbon–carbon bonds that is typical for organic polymer (Prime et al., 2009). At lower temperature, thermal degradation of polymers is initiated at weak link sites. As the temperature goes higher, random scission of polymer chain takes place that gives rise to higher degradation rate and greater extent of degraded products(Prime et al., 2009).
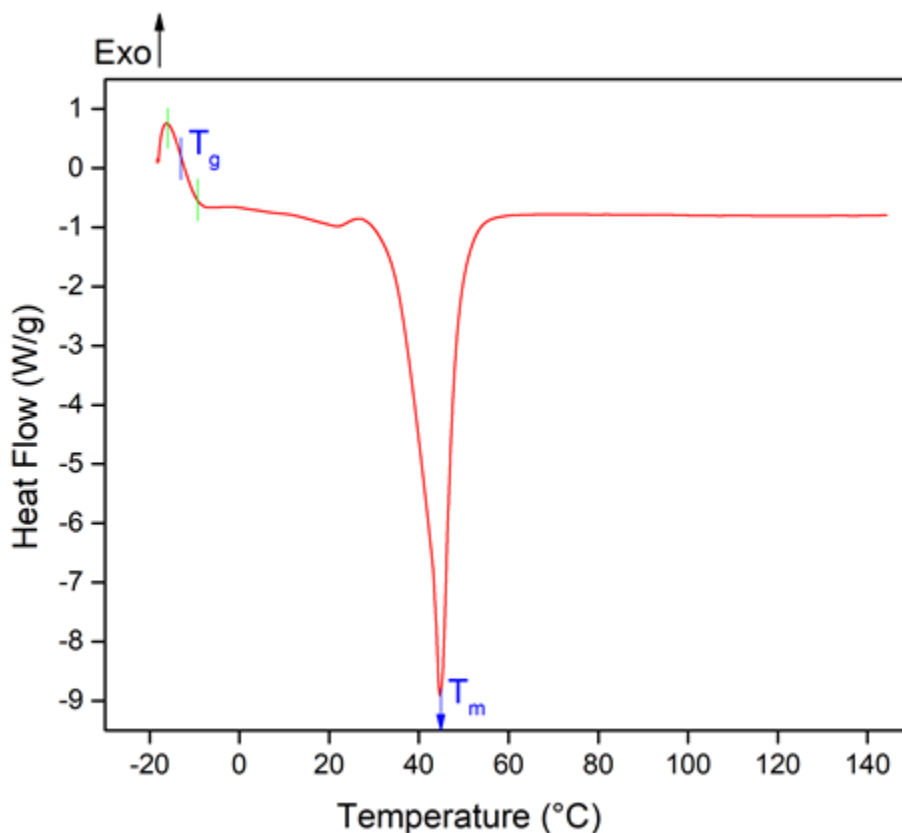
Figure 3.14: DSC analysis for polyester obtained from 9-octadecene-1,18-diester and 9-octadecene-1,18-diol

Glass transition temperature (Tg) and melting temperature (Tm) are key parameters for polymer processing. Below Tg, polymers are rigid (glassy state) and there were no segmental motions possible. The glassy state that is characterized by a small free volume, only allows for local motions of the chain segments(Guigo et al., 2019). As the temperature rises, motions increase with increasing temperature and the material exhibits molecular motions, initiating translational motion of the segments and eventually of the whole chain. The polyester synthesized by using antimony oxide exhibited glass transition temperature (mid Tg) of -12.1°C where the onset Tg and offset Tg were determined to be -16.1°C and -8.1°C respectively as highlighted in Figure 3.14. The prepared polyester demonstrated melting temperatures (Tm) of 44.72 °C. The enthalpy of fusion (ΔH_m) of polyester was also determined from DSC and it was calculated as 83.02 J/g.

After the evaluation of thermal and chemical characteristics, the next step was to prepare films using compression moulding and injection moulding techniques.

A   B
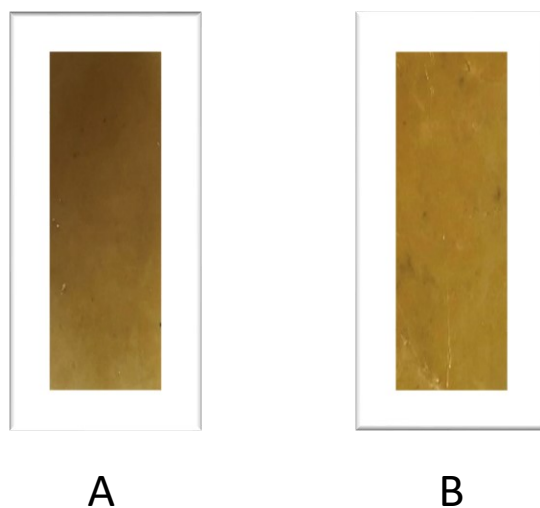
Figure 3.15: A) without Krapton film, B) with Krapton film

For polyester film preparation, the polyesters (~1.5 g) were crushed in a mortar and then taken on steel plates for compression molding. A Carver press was used to press the samples, where a pressure of 1000 psi were applied for 10 min. The temperature of upper plate was maintained at 35°C while lower plate was heated to 40°C and plates were covered with the Krapton film to ensure minimal sticking of the material. This approach helped to achieve uniformity in film thickness and lead to protection against film breakage during plate removals. Moreover, the polyimide Krapton film prevented thermal degradation of the polyester film as shown in Figure 3.15.

Moreover, disc shaped, and dumble-bell shaped specimen were prepared using Injection moulding technique as shown in Figure 3.16.
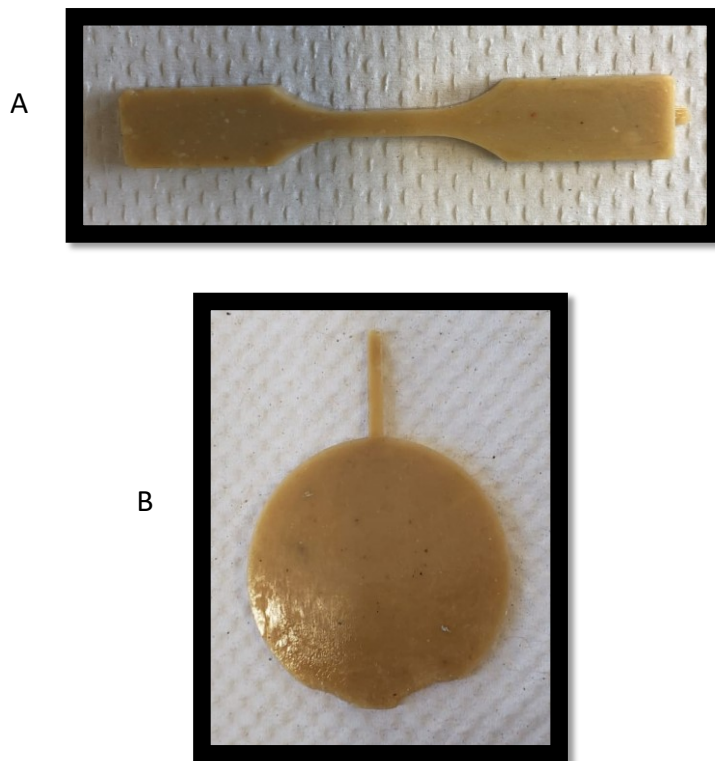
Figure 3.16: Injection moulded samples A) Dumble-bell shaped specimen B) Disc-shaped specimen

Tensile testing was performed for the specimen using Universal Testing machine. The polyester film exhibited tensile strength of 2.44 MPa and 1.14 MPa at yield and breaking point respectively as shown in Figure 3.18. The strain at break was measured as 5.34% while yield strain was found to be 5.14%. The bio-based film demonstrated low Young's modulus of 0.1376 GPa.

A   B
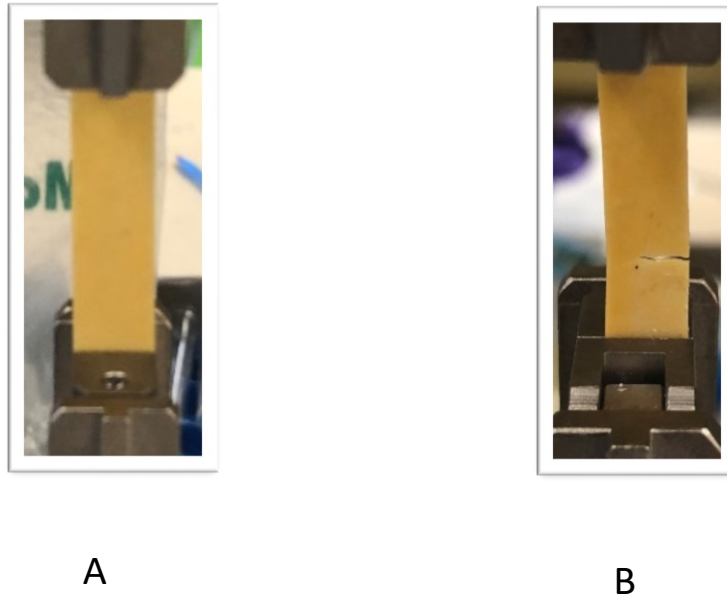
Figure 3.17: Tensile testing of the prepared film A) Mounted sample B) Sample after break
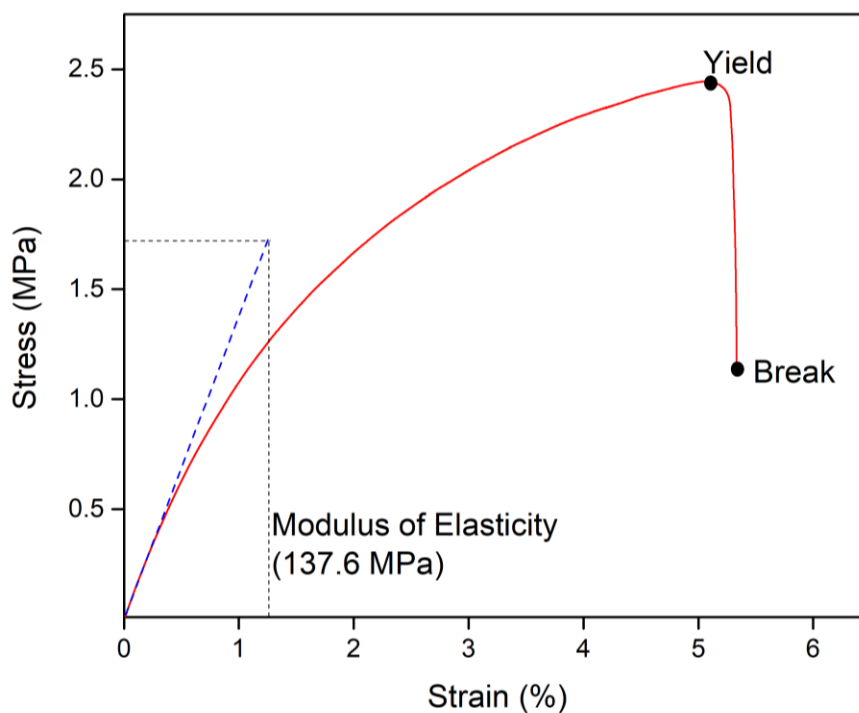
Figure 3.18: Tensile properties of the prepared polyester film

3.3.5 Addition of 3,4-Bis(hydroxymethyl)furan to aliphatic polyester to introduce aromaticity

To introduce aromaticity into the main chain of polyester, 0.23g of 3,4-Bis(hydroxymethyl)furan was added along with 3g of 9-octadecene-1,18-diester and 2.13g 9-octadecene-1,18-diol (molar ratio highlighted in Table 3.1). Partially aromatic polyester was thus synthesized using condensation polymerization technique by incorporating antimony oxide as a catalyst. The condensation reaction was performed in a 25 mL dry round bottom flask for 2 hours at 80°C, after purging the reaction mixture with nitrogen for 15 min. The reaction vial was finally heated to 210 °C under vacuum to initiate polymerization. The reaction was performed for the duration of 4 hours. The viscous nature of the synthesised polymer was marked by observing change in the rate of stirring. The reaction flask was exposed to air followed by precipitation in cold methanol at

least three times (from THF solution) to remove remaining monomer and all other impurities. The collected polymer was dried in a vacuum oven (25 mm Hg) at room temperature to obtain brownish sticky polymer with ~25% yield. The introduction of aromaticity to polyester main chain was confirmed with the help of FTIR.

Table 3.1: Composition of monomers and catalyst used to prepare partially aromatic polyester

	9-octadecene-1,18-diester	9-octadecene-1,18-diol	3,4-Bis(hydroxymethyl) furan	Antimony oxide
Mass (g)	3	2.13	0.23	0.03
Molar Mass (g)	340.5	300	128.13	291.52
Density (g/ml)			1.248	
Volume (ml)			0.18	
Molar ratio	1	0.8	0.2	0.01
Moles	0.0088	0.0071	0.0018	0.0001

As shown in Figure 3.19, absorbance between 1150-1220 cm^{-1} was attributed to C-O-C stretching of polyester. The -OH stretch peak at 3310 cm^{-1} was not observed in polyester spectra that signifies consumption of most diol moieties and it also manifest effectiveness of the washing step. Moreover, stretching band due to carbonyl entity (C=O stretch) was observed at 1728 cm^{-1} that indicates the formation of polyester. The aliphatic C-H stretches from olefinic main chains were observed at 2922 and 2855 cm^{-1}. In addition, the absorbance for C-H bending was also observed at 1409 cm^{-1}. Furthermore, the peak observed between 1550-1600 cm^{-1} corresponds to C=C stretch from aromatic alkene that confirmed incorporation of 3,4-Bis(hydroxymethyl)furan moieties into the main chain of polyester, as also evident in other furan based polyester(Gomes et al., 2011; Howell & Lazar, 2018).
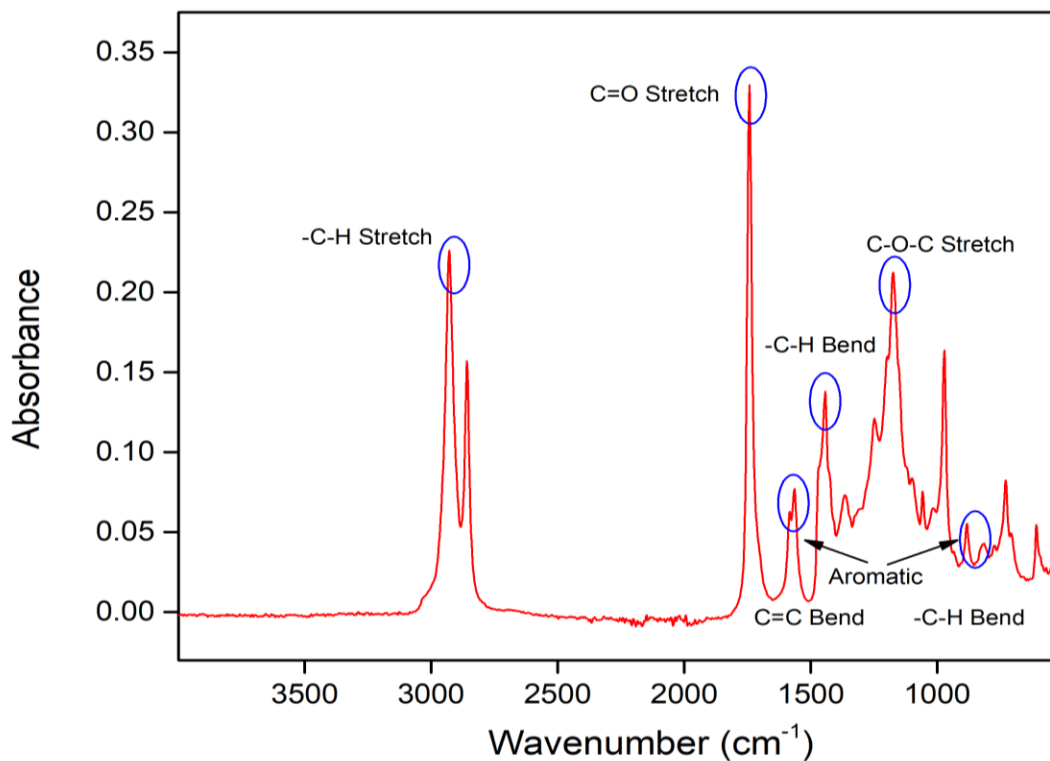
Figure 3.19: ATR-FTIR spectra for polyester synthesized from 9-octadecene-1,18-diester, 9-octadecene-1,18-diol and 3,4-Bis(hydroxymethyl)furan

3.4 Conclusion and future recommendations

To conclude, the valuable feedstock of CF esters has been explored for the first time to obtain polymer precursors using an atom-efficient and solvent-less ethenolysis reaction. An environmentally benign method to develop polymer precursors was successfully employed that demonstrated excellent turnover number values for the ethenolysis of CO (TONs= 92000), UCO (TONs= 78080) and CF (TONs=21820) esters using microwave technology. The synthesis method involved no use of toxic solvents and possessed adequate turnover numbers without encompassing extensive purification of substrates and catalysts. These remarkable results indicate potential utilization of UCO and CF waste resources to substitute petroleum oil-based precursors. This work,

based on rapid synthesis and greener approach opened a new horizon for sustainable production of bio-based polymer precursors from unused, unexplored, yet highly promising lipidic feedstock. Subsequently, the monomer (9-octadecene-1,18-diester) synthesized in the first study was used as a bio-based feedstock to develop polymer that was successfully compression moulded and injection moulded to prepare films and thick specimen. The synthesis method involved no use of toxic solvents and the reaction was carried out using bulk polymerization technique. These results indicated potential utilization of bio-based monomers to substitute petroleum oil-based precursors. However, the mechanical properties were found to be substantially less than that of fossil-based counterparts. Therefore, effort was made to incorporate another bio-based aromatic molecule (3,4-Bis(hydroxymethyl)furan) to enhance its properties. The successful incorporation of aromatic alcohol was confirmed with ATR-FTIR. Due to high cost of (3,4-Bis(hydroxymethyl)furan), only 10% was added for the preparation of polyester. To sum up, the present work, based on the principle of green chemistry and circular economy, could further advance sustainable large-scale production of bio-based polymers thereby complementing environmental sustainability.

The limitation of the current study is low strength and substantially low thermal characteristics as compared to conventional commercialized polymers like PET. Therefore, further optimization of temperature, catalyst as well as feedstock system needs to be catered in future studies. Even though furan ring is more reactive than benzene ring, the use of melt polymerization and high-temperature thermal processing of bio-derived diesters with furan-based diol exhibited low yield, possibly due to less stable furan ring. Hereby, it is postulated that the high-strength polymer can be obtained by using 9-octadecene-1,18-diol with either 2,5-Furandicarboxylic acid or dimethyl 2,5-furandicarboxylate. The employment of highly stable furan-based diester would drastically improve the physiochemical characteristics like glass transition temperature, melting point, tensile

modulus, tensile stress as well as the gas permeability characteristics. Several other catalysts like Germanium oxide or Titanium (IV) alkoxides can also be employed to further achieve high molecular weight polymers. It is expected that the desired results for soft packaging applications could be achieved by implementing these strategies.

References

1. Ray, S., Miglani, S. 2018. Global value chains and the missing links: Cases from Indian industry. Taylor & Francis.

2. Gautam, A.M., Caetano, N. 2017. Study, design and analysis of sustainable alternatives to plastic takeaway cutlery and crockery. Energy Procedia, 136, 507-512.

3. Aljarilla Jimenez, A.I. 2010. *Moldes quirales derivados del norborneno: aplicaciones en reacciones de metátesis*. Universidad Complutense de Madrid, Servicio de Publicaciones.

4. Auras, R., Harte, B., Selke, S. 2004. An overview of polylactides as packaging materials. *Macromolecular bioscience*, **4**(9), 835-864.

5. Bidange, J., Fischmeister, C., Bruneau, C. 2016. Ethenolysis: A Green Catalytic Tool to Cleave Carbon–Carbon Double Bonds. *Chemistry–A European Journal*, **22**(35), 12226-12244.

6. Bogdal, D., Prociak, A. 2008. *Microwave-enhanced polymer chemistry and technology*. John Wiley & Sons.

7. Brent, J. 2001. Current management of ethylene glycol poisoning. *Drugs*, **61**(7), 979-988.

8. Burdett, K.A., Harris, L.D., Margl, P., Maughon, B.R., Mokhtar-Zadeh, T., Saucier, P.C., Wasserman, E.P. 2004. Renewable monomer feedstocks via olefin metathesis:

Fundamental mechanistic studies of methyl oleate ethenolysis with the first-generation Grubbs catalyst. *Organometallics*, **23**(9), 2027-2047.

9.   Chegolya, A., Shevchenko, V., Mikhailov, G. 1979. The formation of polyethylene terephthalate in the presence of dicarboxylic acids. *Journal of Polymer Science: Polymer Chemistry Edition*, **17**(3), 889-904.

10.   Ciriminna, R., Lomeli-Rodriguez, M., Cara, P.D., Lopez-Sanchez, J.A., Pagliaro, M. 2014. Limonene: a versatile chemical of the bioeconomy. *Chemical Communications*, **50**(97), 15288-15296.

11.   De Clercq, R., Dusselier, M., Sels, B. 2017. Heterogeneous catalysis for bio-based polyester monomers from cellulosic biomass: advances, challenges and prospects. *Green Chemistry*, **19**(21), 5012-5040.

12.   Dragutan, V., Demonceau, A., Dragutan, I. 2010. A Selective Route for Synthesis of Linear Polydicyclopentadiene [M], Green Metathesis Chemistry, Springer Netherlands, Rumania.

13.   Duan, B., Huang, Y., Lu, A., Zhang, L. 2018. Recent advances in chitin based materials constructed via physical methods. *Progress in Polymer Science*, **82**, 1-33.

14.   Dutta, P.K. 2016. *Chitin and chitosan for regenerative medicine*. Springer.

15.   Ellis, W.C., Jung, Y., Mulzer, M., Di Girolamo, R., Lobkovsky, E.B., Coates, G.W. 2014. Copolymerization of CO 2 and meso epoxides using enantioselective β-diiminate catalysts: a route to highly isotactic polycarbonates. *Chemical Science*, **5**(10), 4004-4011.

16. Gandini, A. 2011. The irruption of polymers from renewable resources on the scene of macromolecular science and technology. *Green Chemistry*, **13**(5), 1061-1083.

17. Gandini, A., Silvestre, A.J., Neto, C.P., Sousa, A.F., Gomes, M. 2009. The furan counterpart of poly (ethylene terephthalate): An alternative material based on renewable resources. *Journal of Polymer Science Part A: Polymer Chemistry*, **47**(1), 295-298.

18. Gümther, B., Zachmann, H.G. 1983. Influence of molar mass and catalysts on the kinetics of crystallization and on the orientation of poly (ethylene terephthalate). *Polymer*, **24**(8), 1008-1014.

19. Hauenstein, O., Reiter, M., Agarwal, S., Rieger, B., Greiner, A. 2016. Bio-based polycarbonate from limonene oxide and CO_2 with high molecular weight, excellent thermal resistance, hardness and transparency. *Green Chemistry*, **18**(3), 760-770.

20. Hong, S.H., Wenzel, A.G., Salguero, T.T., Day, M.W., Grubbs, R.H. 2007. Decomposition of ruthenium olefin metathesis catalysts. *Journal of the American Chemical Society*, **129**(25), 7961-7968.

21. Inkinen, S., Hakkarainen, M., Albertsson, A.-C., Södergård, A. 2011. From lactic acid to poly (lactic acid)(PLA): characterization and analysis of PLA and its precursors. *Biomacromolecules*, **12**(3), 523-532.

22. Lee, S.H., Cyriac, A., Jeon, J.Y., Lee, B.Y. 2012. Preparation of thermoplastic polyurethanes using in situ generated poly (propylene carbonate)-diols. *Polymer Chemistry*, **3**(5), 1215-1220.

23. MacDonald, W.A. 2002. New advances in poly (ethylene terephthalate) polymerization and degradation. *Polymer International*, **51**(10), 923-930.

24. Maisonneuve, L., Lebarbé, T., Grau, E., Cramail, H. 2013. Structure–properties relationship of fatty acid-based thermoplastics as synthetic polymer mimics. *Polymer Chemistry*, **4**(22), 5472-5517.

25. Meier, M.A., Metzger, J.O., Schubert, U.S. 2007. Plant oil renewable resources as green alternatives in polymer science. *Chemical Society Reviews*, **36**(11), 1788-1802.

26. Papageorgiou, G.Z., Tsanaktsis, V., Bikiaris, D.N. 2014. Synthesis of poly (ethylene furandicarboxylate) polyester using monomers derived from renewable resources: thermal behavior comparison with PET and PEN. *Physical Chemistry Chemical Physics*, **16**(17), 7946-7958.

27. Ren, W.-M., Liu, Z.-W., Wen, Y.-Q., Zhang, R., Lu, X.-B. 2009. Mechanistic aspects of the copolymerization of CO2 with epoxides using a thermally stable single-site cobalt (III) catalyst. *Journal of the American Chemical Society*, **131**(32), 11509-11518.

28.   Shah, T., Bhatty, J., Gamlen, G., Dollimore, D. 1984. Aspects of the chemistry of poly (ethylene terephthalate): 5. Polymerization of bis (hydroxyethyl) terephthalate by various metallic catalysts. *Polymer*, **25**(9), 1333-1336.

29.   Spekreijse, J., Sanders, J.P., Bitter, J.H., Scott, E.L. 2017. The future of ethenolysis in biobased chemistry. *ChemSusChem*, **10**(3), 470-482.

30.   Stahel, W.R. 2019. *The Circular Economy. 1st Edition ed*. Routledge, London.

31.   Stempfle, F., Ortmann, P., Mecking, S. 2016. Long-chain aliphatic polymers to bridge the gap between semicrystalline polyolefins and traditional polycondensates. *Chemical reviews*, **116**(7), 4597-4641.

32.   Thurier, C., Fischmeister, C., Bruneau, C., Olivier-Bourbigou, H., Dixneuf, P.H. 2008. Ethenolysis of methyl oleate in room-temperature ionic liquids. *ChemSusChem: Chemistry & Sustainability Energy & Materials*, **1**(1-2), 118-122.

33.   Ulman, M., Grubbs, R.H. 1999. Ruthenium carbene-based olefin metathesis initiators: catalyst decomposition and longevity. *The Journal of organic chemistry*, **64**(19), 7202-7207.

34.   Wilbon, P.A., Chu, F., Tang, C. 2013. Progress in renewable polymers from natural terpenes, terpenoids, and rosin. *Macromolecular rapid communications*, **34**(1), 8-37.

35. Zhu, C., Zhang, Z., Liu, Q., Wang, Z., Jin, J. 2003. Synthesis and biodegradation of aliphatic polyesters from dicarboxylic acids and diols. *Journal of applied polymer science*, **90**(4), 982-990.

36. 1. Merli, R., M. Preziosi, and A. Acampora, *How do scholars approach the circular economy? A systematic literature review.* Journal of Cleaner Production, 2018. **178**: p. 703-722.

37. 2. Maddikeri, G.L., A.B. Pandit, and P.R. Gogate, *Intensification approaches for biodiesel synthesis from waste cooking oil: a review.* Industrial & Engineering Chemistry Research, 2012. **51**(45): p. 14610-14628.

38. 3. Math, M., S.P. Kumar, and S.V. Chetty, *Technologies for biodiesel production from used cooking oil—A review.* Energy for sustainable Development, 2010. **14**(4): p. 339-345.

39. 4. *Environmental Audit Committee - Green Economy: Written evidence submitted by the UK Sustainable Biodiesel Alliance*2012; Available from:https://publications.parliament.uk/pa/cm201012/cmselect/cmenvaud/1025/1025vw08.htm.

40. 5. Safder, M., F. Temelli, and A. Ullah, *Extraction, optimization, and characterization of lipids from spent hens: An unexploited sustainable bioresource.* Journal of Cleaner Production, 2019. **206**: p. 622-630.

41. 6. Jessop, P., et al., *Opportunities for greener alternatives in chemical formulations.* Green Chemistry, 2015. **17**(5): p. 2664-2678.

42.   7.   Ullah, A. and M. Arshad, *Remarkably Efficient Microwave-Assisted Cross-Metathesis of Lipids under Solvent-Free Conditions.* ChemSusChem, 2017. **10**(10): p. 2167-2174.

43.   8.   Mol, J., *Metathesis of unsaturated fatty acid esters and fatty oils.* Journal of molecular catalysis, 1994. **90**(1-2): p. 185-199.

44.   9.   Chatterjee, A. and V.R. Jensen, *A heterogeneous catalyst for the transformation of fatty acids to α-olefins.* ACS Catalysis, 2017. **7**(4): p. 2543-2547.

45.   10.   Nieres, P., et al., *Heterogeneous catalysis for valorisation of vegetable oils via metathesis reactions: ethenolysis of methyl oleate.* Catalysis Science & Technology, 2016. **6**(17): p. 6561-6568.

46.   11.   Spekreijse, J., et al., *Simultaneous production of biobased styrene and acrylates using ethenolysis.* Green Chemistry, 2012. **14**(10): p. 2747-2751.

47.   12.   Park, C.P., et al., *Low pressure ethenolysis of renewable methyl oleate in a microchemical system.* Organic letters, 2011. **13**(9): p. 2398-2401.

48.   13.   Song, J., et al., *Effect of phase behavior on the ethenolysis of ethyl oleate in compressed CO2.* The Journal of Physical Chemistry B, 2009. **113**(9): p. 2810-2814.

49.   14.   Ashworth, I.W., et al., *Olefin metathesis by grubbs–hoveyda complexes: computational and experimental studies of the mechanism and substrate-dependent kinetics.* Acs Catalysis, 2013. **3**(9): p. 1929-1939.

50.   15.   Burdett, K.A., et al., *Renewable monomer feedstocks via olefin metathesis: Fundamental mechanistic studies of methyl oleate ethenolysis with the first-generation Grubbs catalyst.* Organometallics, 2004. **23**(9): p. 2027-2047.

51.   16.   Arshad, M., S. Saied, and A. Ullah, *PEG–lipid telechelics incorporating fatty acids from canola oil: synthesis, characterization and solution self-assembly.* RSC Advances, 2014. **4**(50): p. 26439-26446.

52.   Aljarilla Jiménez, A.I. 2010. *Moldes quirales derivados del norborneno: aplicaciones en reacciones de metátesis*. Universidad Complutense de Madrid, Servicio de Publicaciones.

53.   Auras, R., Harte, B., Selke, S. 2004. An overview of polylactides as packaging materials. *Macromolecular bioscience*, **4**(9), 835-864.

54.   Bidange, J., Fischmeister, C., Bruneau, C. 2016. Ethenolysis: A Green Catalytic Tool to Cleave Carbon–Carbon Double Bonds. *Chemistry–A European Journal*, **22**(35), 12226-12244.

55.   Bogdal, D., Prociak, A. 2008. *Microwave-enhanced polymer chemistry and technology*. John Wiley & Sons.

56.   Brent, J. 2001. Current management of ethylene glycol poisoning. *Drugs*, **61**(7), 979-988.

57.   Burdett, K.A., Harris, L.D., Margl, P., Maughon, B.R., Mokhtar-Zadeh, T., Saucier, P.C., Wasserman, E.P. 2004. Renewable monomer feedstocks via olefin metathesis: Fundamental mechanistic studies of methyl oleate ethenolysis with the first-generation Grubbs catalyst. *Organometallics*, **23**(9), 2027-2047.

58.   Burgess, S.K., Leisen, J.E., Kraftschik, B.E., Mubarak, C.R., Kriegel, R.M., Koros, W.J. 2014. Chain mobility, thermal, and mechanical properties of poly (ethylene furanoate) compared to poly (ethylene terephthalate). *Macromolecules*, **47**(4), 1383-1391.

59. Caillol, S., Desroches, M., Boutevin, G., Loubat, C., Auvergne, R., Boutevin, B. 2012. Synthesis of new polyester polyols from epoxidized vegetable oils and biobased acids. *European Journal of Lipid Science and Technology*, **114**(12), 1447-1459.

60. Chegolya, A., Shevchenko, V., Mikhailov, G. 1979. The formation of polyethylene terephthalate in the presence of dicarboxylic acids. *Journal of Polymer Science: Polymer Chemistry Edition*, **17**(3), 889-904.

61. Ciriminna, R., Lomeli-Rodriguez, M., Cara, P.D., Lopez-Sanchez, J.A., Pagliaro, M. 2014. Limonene: a versatile chemical of the bioeconomy. *Chemical Communications*, **50**(97), 15288-15296.

62. Dai, J., Ma, S., Liu, X., Han, L., Wu, Y., Dai, X., Zhu, J. 2015. Synthesis of bio-based unsaturated polyester resins and their application in waterborne UV-curable coatings. *Progress in Organic Coatings*, **78**, 49-54.

63. De Clercq, R., Dusselier, M., Sels, B. 2017. Heterogeneous catalysis for bio-based polyester monomers from cellulosic biomass: advances, challenges and prospects. *Green Chemistry*, **19**(21), 5012-5040.

64. Dragutan, V., Demonceau, A., Dragutan, I. 2010. A Selective Route for Synthesis of Linear Polydicyclopentadiene [M], Green Metathesis Chemistry, Springer Netherlands, Rumania.

65. Duan, B., Huang, Y., Lu, A., Zhang, L. 2018. Recent advances in chitin based materials constructed via physical methods. *Progress in Polymer Science*, **82**, 1-33.

66. Dutta, P.K. 2016. *Chitin and chitosan for regenerative medicine*. Springer.

67. Elliot, S.G., Andersen, C., Tolborg, S., Meier, S., Sádaba, I., Daugaard, A.E., Taarning, E. 2017. Synthesis of a novel polyester building block from pentoses by tin-containing silicates. *Rsc Advances*, **7**(2), 985-996.

68.   Ellis, W.C., Jung, Y., Mulzer, M., Di Girolamo, R., Lobkovsky, E.B., Coates, G.W. 2014. Copolymerization of CO 2 and meso epoxides using enantioselective β-diiminate catalysts: a route to highly isotactic polycarbonates. *Chemical Science*, **5**(10), 4004-4011.

69.   Fodor, C., Golkaram, M., Woortman, A.J., van Dijken, J., Loos, K. 2017. Enzymatic approach for the synthesis of biobased aromatic–aliphatic oligo-/polyesters. *Polymer Chemistry*, **8**(44), 6795-6805.

70.   Gandini, A. 2011. The irruption of polymers from renewable resources on the scene of macromolecular science and technology. *Green Chemistry*, **13**(5), 1061-1083.

71.   Gandini, A., Silvestre, A.J., Neto, C.P., Sousa, A.F., Gomes, M. 2009. The furan counterpart of poly (ethylene terephthalate): An alternative material based on renewable resources. *Journal of Polymer Science Part A: Polymer Chemistry*, **47**(1), 295-298.

72.   Gautam, A.M., Caetano, N. 2017. Study, design and analysis of sustainable alternatives to plastic takeaway cutlery and crockery. *Energy Procedia*, **136**, 507-512.

73.   Gomes, M., Gandini, A., Silvestre, A.J., Reis, B. 2011. Synthesis and characterization of poly (2, 5-furan dicarboxylate) s based on a variety of diols. *Journal of Polymer Science Part A: Polymer Chemistry*, **49**(17), 3759-3768.

74.   Guigo, N., Forestier, E., Sbirrazzuoli, N. 2019. Thermal Properties of Biobased Polymers: Furandicarboxylic Acid (FDCA)-Based Polyesters.

75.   Gümther, B., Zachmann, H.G. 1983. Influence of molar mass and catalysts on the kinetics of crystallization and on the orientation of poly (ethylene terephthalate). *Polymer*, **24**(8), 1008-1014.

76. Haq, M., Burgueño, R., Mohanty, A.K., Misra, M. 2009. Bio-based unsaturated polyester/layered silicate nanocomposites: Characterization and thermo-physical properties. *Composites Part A: Applied Science and Manufacturing*, **40**(4), 540-547.

77. Haq, M., Burgueño, R., Mohanty, A.K., Misra, M. 2008. Hybrid bio-based composites from blends of unsaturated polyester and soybean oil reinforced with nanoclay and natural fibers. *Composites Science and Technology*, **68**(15-16), 3344-3351.

78. Hauenstein, O., Reiter, M., Agarwal, S., Rieger, B., Greiner, A. 2016. Bio-based polycarbonate from limonene oxide and CO 2 with high molecular weight, excellent thermal resistance, hardness and transparency. *Green Chemistry*, **18**(3), 760-770.

79. Hong, S.H., Wenzel, A.G., Salguero, T.T., Day, M.W., Grubbs, R.H. 2007. Decomposition of ruthenium olefin metathesis catalysts. *Journal of the American Chemical Society*, **129**(25), 7961-7968.

80. Howell, B.A., Lazar, S.T. 2018. Biobased plasticizers from carbohydrate-derived 2, 5-bis (hydroxymethyl) furan. *Industrial & Engineering Chemistry Research*, **58**(3), 1222-1228.

81. Inkinen, S., Hakkarainen, M., Albertsson, A.-C., Södergård, A. 2011. From lactic acid to poly (lactic acid)(PLA): characterization and analysis of PLA and its precursors. *Biomacromolecules*, **12**(3), 523-532.

82. Jiang, Y., Woortman, A.J., Alberda van Ekenstein, G.O., Petrović, D.M., Loos, K. 2014. Enzymatic synthesis of biobased polyesters using 2, 5-bis (hydroxymethyl) furan as the building block. *Biomacromolecules*, **15**(7), 2482-2493.

83. Le Roux, E. 2016. Recent advances on tailor-made titanium catalysts for biopolymer synthesis. *Coordination Chemistry Reviews*, **306**, 65-85.

84. Lee, S.H., Cyriac, A., Jeon, J.Y., Lee, B.Y. 2012. Preparation of thermoplastic polyurethanes using in situ generated poly (propylene carbonate)-diols. *Polymer Chemistry*, **3**(5), 1215-1220.

85. Li, H., He, G., Chen, Y., Zhao, J., Zhang, G. 2019. One-Step Approach to Polyester–Polyether Block Copolymers Using Highly Tunable Bicomponent Catalyst. *ACS Macro Letters*, **8**(8), 973-978.

86. Liu, C., Li, J., Lei, W., Zhou, Y. 2014. Development of biobased unsaturated polyester resin containing highly functionalized castor oil. *Industrial crops and products*, **52**, 329-337.

87. MacDonald, W.A. 2002. New advances in poly (ethylene terephthalate) polymerization and degradation. *Polymer International*, **51**(10), 923-930.

88. Maisonneuve, L., Lebarbé, T., Grau, E., Cramail, H. 2013. Structure–properties relationship of fatty acid-based thermoplastics as synthetic polymer mimics. *Polymer Chemistry*, **4**(22), 5472-5517.

89. Meier, M.A., Metzger, J.O., Schubert, U.S. 2007. Plant oil renewable resources as green alternatives in polymer science. *Chemical Society Reviews*, **36**(11), 1788-1802.

90. Papageorgiou, G.Z., Tsanaktsis, V., Bikiaris, D.N. 2014. Synthesis of poly (ethylene furandicarboxylate) polyester using monomers derived from renewable resources: thermal behavior comparison with PET and PEN. *Physical Chemistry Chemical Physics*, **16**(17), 7946-7958.

91. Pellis, A., Acero, E.H., Ferrario, V., Ribitsch, D., Guebitz, G.M., Gardossi, L. 2016. The closure of the cycle: enzymatic synthesis and functionalization of bio-based polyesters. *Trends in biotechnology*, **34**(4), 316-328.

92.   Prime, R.B., Bair, H.E., Vyazovkin, S., Gallagher, P.K., Riga, A. 2009. Thermogravimetric analysis (TGA). *Thermal analysis of polymers: Fundamentals and applications*, 241-317.

93.   Quinzler, D., Mecking, S. 2010. Linear semicrystalline polyesters from fatty acids by complete feedstock molecule utilization. *Angewandte Chemie International Edition*, **49**(25), 4306-4308.

94.   Ray, S., Miglani, S. 2018. *Global value chains and the missing links: Cases from Indian industry*. Taylor & Francis.

95.   Ren, W.-M., Liu, Z.-W., Wen, Y.-Q., Zhang, R., Lu, X.-B. 2009. Mechanistic aspects of the copolymerization of CO2 with epoxides using a thermally stable single-site cobalt (III) catalyst. *Journal of the American Chemical Society*, **131**(32), 11509-11518.

96.   Shah, T., Bhatty, J., Gamlen, G., Dollimore, D. 1984. Aspects of the chemistry of poly (ethylene terephthalate): 5. Polymerization of bis (hydroxyethyl) terephthalate by various metallic catalysts. *Polymer*, **25**(9), 1333-1336.

97.   Sousa, A.F., Vilela, C., Fonseca, A.C., Matos, M., Freire, C.S., Gruter, G.-J.M., Coelho, J.F., Silvestre, A.J. 2015. Biobased polyesters and other polymers from 2, 5-furandicarboxylic acid: a tribute to furan excellency. *Polymer chemistry*, **6**(33), 5961-5983.

98.   Spekreijse, J., Sanders, J.P., Bitter, J.H., Scott, E.L. 2017. The future of ethenolysis in biobased chemistry. *ChemSusChem*, **10**(3), 470-482.

99.   Stahel, W.R. 2019. *The Circular Economy*. *1st Edition ed*. Routledge, London.

100.   Stempfle, F., Ortmann, P., Mecking, S. 2016. Long-chain aliphatic polymers to bridge the gap between semicrystalline polyolefins and traditional polycondensates. *Chemical reviews*, **116**(7), 4597-4641.

101. Thurier, C., Fischmeister, C., Bruneau, C., Olivier-Bourbigou, H., Dixneuf, P.H. 2008. Ethenolysis of methyl oleate in room-temperature ionic liquids. *ChemSusChem: Chemistry & Sustainability Energy & Materials*, **1**(1-2), 118-122.

102. Ulman, M., Grubbs, R.H. 1999. Ruthenium carbene-based olefin metathesis initiators: catalyst decomposition and longevity. *The Journal of organic chemistry*, **64**(19), 7202-7207.

103. Vyazovkin, S. 2002. Thermogravimetric analysis. *Characterization of Materials*, 1-12.

104. Wilbon, P.A., Chu, F., Tang, C. 2013. Progress in renewable polymers from natural terpenes, terpenoids, and rosin. *Macromolecular rapid communications*, **34**(1), 8-37.

105. Zhu, C., Zhang, Z., Liu, Q., Wang, Z., Jin, J. 2003. Synthesis and biodegradation of aliphatic polyesters from dicarboxylic acids and diols. *Journal of applied polymer science*, **90**(4), 982-990.